Space Science Reviews (2024) 220:58
https://doi.org/10.1007/s11214-024-01087-w

Strong Gravitational Lensing as a Probe of Dark Matter

S. Vegetti[1] · S. Birrer[2] · G. Despali[3,4] · C.D. Fassnacht[5] · D. Gilman[6] · Y. Hezaveh[7,8,9,10,11] · L. Perreault Levasseur[7,8,9,10,11] · J.P. McKean[12,13,14] · D.M. Powell[1] · C.M. O'Riordan[1] · G. Vernardos[15]

Received: 17 June 2023 / Accepted: 1 July 2024

Abstract
Dark matter structures within strong gravitational lens galaxies and along their lines of sight leave a gravitational imprint on the multiple images of lensed sources. Strong gravitational lensing provides, therefore, a key test of different dark matter models. In this article, we describe how galaxy-scale strong gravitational lensing observations are sensitive to the physical nature of dark matter. We provide an historical perspective of the field, and review its current status. We discuss the challenges and advances in terms of data, treatment of systematic errors and theoretical predictions, that will enable one to deliver a stringent and robust test of different dark matter models in the next decade. With the advent of the next generation of sky surveys, the number of known strong gravitational lens systems is expected to increase by several orders of magnitude. Coupled with high-resolution follow-up observations, these data will provide a key opportunity to constrain the properties of dark matter with strong gravitational lensing.

Keywords Gravitational lensing: strong · Haloes: number · Structure · Dark matter

1 Introduction

In the standard cosmological model, 85 per cent of the total amount of matter in the Universe is made of non-baryonic dark matter (Planck Collaboration et al. 2020b). Evidence of the existence of dark matter spans a wide range of independent astronomical observations: the cosmic micro-wave background (Planck Collaboration et al. 2020a), the rotation curves of disk galaxies (e.g. van Albada et al. 1985; Rubin 1991), the motion of galaxies within clusters (e.g. Zwicky 1933), gravitational lensing by galaxies and galaxy clusters (e.g Treu and Koopmans 2004; Mandelbaum et al. 2006; Clowe et al. 2006; Auger et al. 2009; Barnabè et al. 2011; Sonnenfeld et al. 2022; Shajib et al. 2024), hot gas in galaxy clusters (e.g. Ettori et al. 2013), weak lensing and galaxy clustering (e.g. Alam et al. 2017; Heymans et al. 2021; Abbott et al. 2022). To this day, the physical nature of dark matter remains an unsolved problem. There is no dark matter particle within the standard model of particle physics. So far, several candidates, spanning 90 orders of magnitude in mass, have been proposed (Bertone and Tait 2018). In the 1980s, weakly interactive massive particles (WIMPs) emerged as the favourite candidate for cold dark matter. The success of WIMPs stems from the fact that their existence is predicted by Supersymmetry theories (Fox 2018, and references therein),

Extended author information available on the last page of the article

according to which they are thermally produced with a self-interaction cross-section that leads to the correct amount of dark matter at the present day. However, decades of particle physics experiments have failed to produce a WIMP detection (Arcadi et al. 2018).

Other viable dark matter candidates include warm (WDM), self-interacting (SIDM) and fuzzy (FDM) dark matter. We refer the reader to Sect. 2 for a more detailed description of the various models. What makes these alternative models interesting is that they predict a different distribution of dark matter on subgalactic scales.

Strong gravitational lensing is sensitive to the distribution of matter and dark matter between the observer and the source. It is a purely gravitational probe and does not rely on the presence and distribution of baryons. It therefore provides a channel to observationally constrain the physical nature of dark matter. Other probes include the Lyman-α forest (e.g. Villasenor et al. 2023), the satellite galaxies of the Milky Way (e.g. Nadler et al. 2021) and stellar streams in the Local Group (e.g. Erkal et al. 2017).

This article focuses on galaxy-scale strong gravitational lensing as a probe of dark matter and is organized as follows. In Sect. 2, we give a description of the dark matter models that have so far been tested with strong gravitational lensing observations. We expect this list to increase in the future as theoretical predictions for structure formation in more dark matter models become available. In Sect. 3, we discuss how lensing observables (i.e. image positions, fluxes, and time delays) are affected by the distribution of dark matter on small scales. In Sect. 4, we describe the process of lens modelling and how one can constrain the properties of dark matter from strong gravitational lensing observations as an inference problem. Another important aspect is the role played by degeneracies, systematic errors and unknowns, all of which are discussed in Sect. 5. The article then continues with an historical perspective of the field (Sect. 6), its current status (Sect. 7) and how it is likely to evolve in the near future (Sect. 8). We recognize that the last two sections may soon be obsolete. Therefore, we encourage the interested reader to complement this text with the latest relevant publications. Finally, we present our concluding remarks in Sect. 9.

2 Dark Matter Models

We begin this section by introducing theoretical predictions on the properties of low-mass haloes in the CDM model as derived from numerical simulations. Alternative dark matter models can affect both the number and the structural properties of these objects and, as a consequence, the lensing signal that they produce. In the rest of this section, we describe the most studied models and how they differ from CDM. In Sect. 5.6, we discuss current theoretical uncertainties (e.g. the effect of baryons) relative to the subhalo mass function and mass density profile, and how these affect the robustness of dark matter constraints from strong gravitational lensing observations.

2.1 Cold Dark Matter

Dark matter models where the particle is non-relativistic are described as cold. Possible candidates include WIMPs and axions (e.g. Feng 2010). At the same time, dark matter does not have to be a particle and primordial black holes have also been proposed as a CDM candidate (e.g. Green and Kavanagh 2021). Thanks to its several successes at reproducing many observations (especially on large scales), CDM is, at present, the prevailing cosmological model. However, it remains largely untested on subgalactic scales, where strong gravitational lensing represents a key opportunity to further assess its validity. One of the fundamental predictions of CDM is the fact that dark matter structures form hierarchically and

bottom-up: low-mass haloes form first and subsequently merge into structures of increasing mass and size. The structure and evolution of CDM haloes has been extensively studied and precisely characterised using numerical simulations (see Zavala and Frenk 2019, for a review). The collisionless nature of CDM and hierarchical structure formation result in a population of haloes with well defined properties.

Halo mass function: at the low-mass end, the number density n of haloes is well-described, to first approximation, by a power-law distribution:

$$\frac{dn}{dM} \propto M^{-\alpha}\,. \tag{1}$$

For halo masses smaller than a mass of $M \sim 10^{11} M_{\odot}$ the slope is $\alpha = 1.9$, and the number of structures increases with decreasing halo mass. The shape of the halo mass function is well understood from statistical arguments. These are based on the properties of the initial density field of fluctuations and the gravitational collapse process that leads to the formation of virialised haloes. This is at the basis of the formalism first introduced by Press and Schechter (1974), and subsequently extended and improved by Sheth and Tormen (1999), Sheth et al. (2001), Tinker et al. (2008) and Despali et al. (2016).

Subhalo mass function: the number density of haloes that have been accreted onto larger ones is also thought to be a power-law with a normalisation that depends on the host halo mass and redshift (e.g. Gao et al. 2004; Springel et al. 2008; Giocoli et al. 2008; Angulo et al. 2009; Despali and Vegetti 2017). Due to the interaction between the subhaloes and the host, the former are tidally stripped and sometimes destroyed (e.g. Angulo et al. 2009; Berezinsky et al. 2014; Delos 2019; Green and van den Bosch 2019; Green et al. 2021). As a consequence of this process, the total number of subhaloes in hydrodynamical simulations is reduced by between 20 and 50 per cent, depending on the galaxy formation model, relative to dark-matter-only simulations (Sawala et al. 2017; Despali and Vegetti 2017; Chua et al. 2017). The number density of subhaloes also changes as a function of distance from the halo centre according to an Einasto profile (Springel et al. 2008). However, at fixed subhalo mass, the projected number density distribution is constant with radius (Xu et al. 2015; Despali and Vegetti 2017).

Halo mean mass density profile: the mass density $\rho(r)$ of a dark matter halo as a function of radius r is described by the Navarro, Frenk and White profile (NFW, Navarro et al. 1996):

$$\rho(r) = \frac{\rho_s}{\frac{r}{r_s}\left(1+\frac{r}{r_s}\right)^2}\,. \tag{2}$$

Here, r_s is the scale radius and ρ_s is the density normalization. The NFW profile can also be defined in terms of the halo virial mass $M_{\rm vir}$ (i.e. the mass within the radius, $r_{\rm vir}$, that encloses a virial overdensity $\Delta_{\rm vir}$, defined following Bryan and Norman 1998), and the virial concentration $c_{\rm vir} = r_{\rm vir}/r_s$.

Subhalo mean mass density profile: due to the tidal interactions between the subhaloes and the host halo, the mass density profiles of the former tend to deviate from a standard NFW profile and are significantly more concentrated than isolated haloes of the same mass (e.g. Moliné et al. 2017). For this reason, their properties are better described in terms of the peak circular velocity $V_{\rm max}$ and the corresponding $R_{\rm max}$ radius.

2.2 Warm Dark Matter

Dark matter particles with (close to) relativistic free-streaming velocities in the early Universe, for example, light neutrinos, are commonly described as Hot Dark Matter candidates

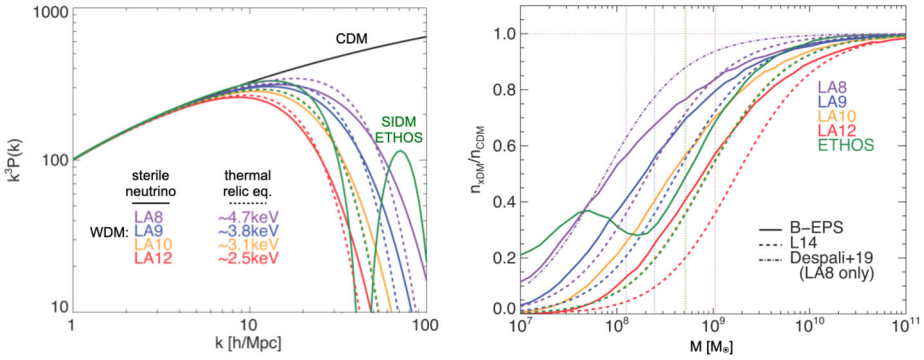

Fig. 1 Power spectra (left) and mass functions (right) in warm and self-interacting dark matter models. In the left panel, the CDM $P(k)$ is shown in black, while different colours represent four WDM models and one SIDM model (ETHOS, see Vogelsberger et al. 2016) in which the power-spectrum is modified. In the WDM case, the suppression is shown both for sterile neutrino models (solid) and their thermal-relic closest counterpart (dashed). The right panel shows instead the suppression in the halo mass function with respect to CDM, calculated with the extended Press-Schechter (EPS) formalism, or measured in simulations (Lovell et al. 2014; Despali et al. 2018). The figures are adapted from Fig. 1 and 2 in Lovell (2020), respectively

(Doroshkevich et al. 1981). A universe predominantly made of HDM has already been ruled out by observations of the clustering of galaxies on large scales (White et al. 1983). Between CDM and HDM lies a class of dark matter models known as warm dark matter (WDM), whose candidates include the gravitino and sterile neutrinos (e.g. Boyarsky et al. 2009, 2019; Paduroiu 2022). They are non-relativistic, but have a non-negligibile free-streaming velocity at early times. This property leads to the suppression of the power-spectrum of the mass-density fluctuations on scales smaller than the half-mode scale $\lambda_{\rm hm}$ (Viel et al. 2012; Iršič et al. 2017) - see Fig. 1. The corresponding suppression in the number density of low-mass haloes relative to CDM can be expressed as follows (Schneider et al. 2012; Lovell et al. 2012; Bose et al. 2016; Lovell 2020):

$$\frac{n_{\rm WDM}}{n_{\rm CDM}} = \left(1 + \gamma \frac{M_{\rm hm}}{M}\right)^{\beta}. \tag{3}$$

$M_{\rm hm}$ is the *half-mode mass* and is defined as the mass-scale at which the square root of the WDM linear matter power-spectrum is 50 per cent smaller than in CDM. In practice, the half-mode mass is inversely proportional to the dark matter particle mass m_{DM}: the lighter the particle candidate, the stronger the suppression in the mass function at small scales.

As a result of the increased particle velocity in WDM, structure formation is delayed to a time when the Universe is less dense. As a consequence, haloes of a given mass are not only less numerous, but also less concentrated (e.g. Ludlow et al. 2016). By suppressing both halo abundance and halo concentration, the latter quantity determining the lensing efficiency of haloes, WDM models predict less small-scale perturbations to the strong gravitationally lensed images than one would expect from CDM (Despali et al. 2018; Li et al. 2017; Despali et al. 2020).

2.3 Self-Interacting Dark Matter

Self-interacting dark matter (SIDM) postulates that dark matter particles are not collisionless, but have non-gravitational interactions in which they exchange energy and momentum.

The term SIDM refers to a variety of models that include elastic or inelastic scattering and a constant or velocity dependent interaction cross-section (Vogelsberger et al. 2012; Rocha et al. 2013; Kaplinghat et al. 2014; Vogelsberger et al. 2016; Sameie et al. 2018; Robertson et al. 2018; Lovell et al. 2019; Kaplinghat et al. 2019; Vogelsberger et al. 2019; Despali et al. 2019; Sameie et al. 2020; Kaplinghat et al. 2020; Robertson et al. 2021; Correa 2021).

The distinctive signature of SIDM is a modification of the central mass density profile of haloes and subhaloes. The interactions between dark matter particles in high-density regions lead to a transfer of heat and the formation of a density core with a depth and size that is related to the strength of the self-interaction cross-section σ. In some cases, however, the halo and subhalo subsequently undergo a runaway contraction, also known as gravo-thermal catastrophe or core collapse. This phenomenon results in the formation of a cuspy density profile. It is accelerated by the presence of baryons (e.g. Feng et al. 2021) and, in the case of subhaloes, by tidal stripping (Nishikawa et al. 2020). From a strong gravitational lensing perspective, these diverse changes to the central mass density distribution imply that certain (sub-)haloes will be more efficient lenses than others (Despali et al. 2019; Robertson et al. 2019; Gilman et al. 2021, 2022; Amorisco et al. 2022).

In addition to altering the internal structure of haloes, SIDM can also suppress the abundance of subhaloes relative to CDM through ram-pressure stripping of the subhaloes while they are accreted by the host galaxy (see Fig. 1) and Nadler et al. 2020; Zeng et al. 2022). As ram-pressure stripping occurs due to self-interactions between dark matter particles (as distinct from baryonic ram-pressure stripping) bound to the subhaloes and those bound to the host, the efficiency of this mechanism depends on the amplitude of the self-interaction cross-section. For example, in velocity-independent SIDM models with elastic scattering, a very high cross-section ($\sigma \sim 10$ cm^2 g^{-1}) is required. These models are currently ruled out by observations of galaxy clusters (Sagunski et al. 2021; Andrade et al. 2022).

Strong gravitational lensing, being sensitive to the amount and concentration of low-mass haloes (i.e. with a central velocity dispersion from less than ~ 10 km s^{-1} to ~ 50 km s^{-1}), provides, therefore, an independent avenue to constrain SIDM models. It allows one to constrain the self-interaction cross-section at low velocities and complements the constraints derived from galaxies and galaxy clusters (e.g. Loudas et al. 2022).

2.4 Fuzzy Dark Matter

Fuzzy dark matter is a particular form of dark matter made of *ultra-light* bosons, i.e., $m_{\rm DM}c^2 \sim 10^{-22}$ eV. This particle mass is orders of magnitude smaller than that of WIMPs and WDM models. As a result, the de Broglie wavelength is larger than the inter-particle separation and waves better describe the behaviour of the FDM field. This effect leads to a series of distinctive phenomenologies with respect to the other dark matter models so far considered (see Hui 2021, for a review). For example, numerical simulations, which model the full non-linear evolution (Schive et al. 2014a; May and Springel 2021), show that the wave-like behaviour (e.g. interference effects) of FDM leads to the formation of a soliton core at the centre of haloes and density granules on scales smaller than a kpc.

Similarly to WDM, there is a cut-off in the FDM transfer function at small scales, though via a different mechanism that is dependent on the de Broglie wavelength rather than a free-streaming length.[1] As a consequence, from a strong gravitational lensing perspective, FDM models are expected to lead to fewer perturbations of the lensed images compared to CDM.

[1] Note, however, that the wave-like nature of ultra-light dark matter particles results in the FDM power-spectrum to briefly exceeds that in CDM on $\mathcal{O}$(kpc) scales that correspond to the mean de Broglie wavelength.

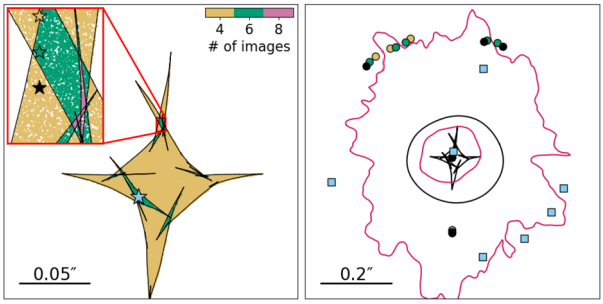

Fig. 2 Lensed image multiplicity in FDM. The left panel shows the caustic structure of a galaxy-scale lens in FDM. The colour indicates the number of lensed images for a point source located at different positions on the source plane. The right panel shows the corresponding lensed image position on the observed plane. Rare hexad and octad images become more likely in FDM models. Figure reproduced with permission from Chan et al. (2020), copyright by APS

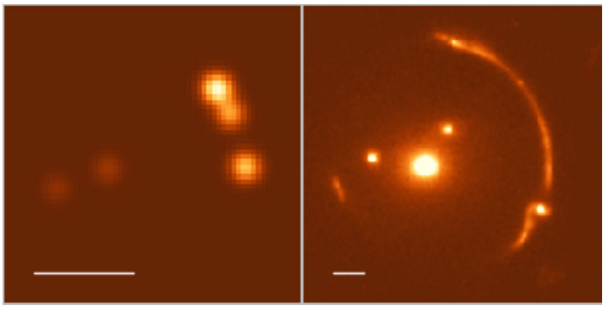

Fig. 3 Two examples of galaxy-scale lenses with a unresolved (left) and resolved (right) background source. On the left panel, the gravitational lens system B2045+265 shows a strong flux-ratio anomaly which is inconsistent with a smooth lens mass distribution (Fassnacht et al. 1999). On the right, the gravitational lens system SDSSJ120602.09+514229.5, also known as the Clone, displays a distorted arc due to the presence of a small luminous satellite galaxy (Vegetti et al. 2010)

However, the granular structure in the halo density profile of lens galaxies has been shown to lead to a distinct new source of small-scale perturbations of the lensed images, which is unique to FDM models (see Fig. 2 and Chan et al. 2020; Laroche et al. 2022; Powell et al. 2023; Amruth et al. 2023).

3 Strong Lensing as a Probe of Dark Matter

Changes to the matter distribution on subgalactic scales within lens galaxies and along their lines of sight leave a gravitational imprint on the strong lensing data. Here, we briefly describe the nature and strength of this effect. In particular, we discuss changes induced on the lensing potential, its first and second derivative, and how they affect the observed time-delay, image positions and magnifications, respectively. For an historical perspective of the field, we refer the reader to Sect. 6.

Image magnification: The largest effect produced by local fluctuations in the lensing mass density distribution (either in the form of subhaloes, field haloes or FDM granules)

is a change in the relative magnification of unresolved lensed images (see Fig. 3 for an example), and the creation of so called flux-ratio anomalies. These anomalies could also be related to micro-lensing by stars (see Chap. 5) or propagation effects such as free-free absorption at long wavelength (Mittal et al. 2007) and dust extinction (Elíasdóttir et al. 2006) in the lens galaxy. The observed ratios are also affected by intrinsic and extrinsic (such as microlensing or interstellar scattering) variability of the background source (Koopmans et al. 2003; Biggs 2023). As such, they can only be used as a probe of dark matter with observations at wavelengths where the angular size of the lensed object is larger than the scale of the micro-lenses, and at which dust and free electron absorption and/or scattering is low. Since flux-ratio anomalies are related to a local change of the second derivative of the lensing potential, they are an effective tool to detect some of the lowest mass perturbations. Lenses with small image separation (relative to the scale of the macro-lens) in the fold and cusp configurations (i.e. where the source lies on the cusp or fold of the caustic curves) are the most sensitive to the perturbations of the lensing potential and least sensitive to intrinsic variability. In these cases, the following $R_{\rm fold}$ and $R_{\rm cusp}$ relations have been sometimes used to quantify the strengths of the anomaly:

$$R_{\rm fold} = \frac{\mu_A + \mu_B}{|\mu_A| + |\mu_B|}, \tag{4}$$

and

$$R_{\rm cusp} = \frac{\mu_B + \mu_A + \mu_c}{|\mu_A| + |\mu_B| + |\mu_C|}. \tag{5}$$

Here, $\mu_{A,B}$ in $R_{\rm fold}$ and $\mu_{A,B,C}$ in $R_{\rm cusp}$ are the magnifications of the merging double and triplet images, respectively. As the opening angles between the images A and C ($\Delta\phi$) in the cusp configuration and A and B (ϕ_1) in the fold configuration approach zero, so do $R_{\rm fold}$ and $R_{\rm cusp}$, when the lens mass distribution is smooth and the background source is a point-source. However, it is worth noting that both relations suffer from a few limitations. First, astrophysical sources of emission, whether they be the accretion disk, the narrow emission line region or the warm (> 50 K) dust torus around a black hole or the relativistic jet that they produce are not point-like, but have some angular scale. Second, the fold relation is only reliable when the image separation is smaller than the distance at which the image with negative parity would have a less than unity magnification. While the cusp relation breaks down unless the source is very close to the bisector.

Image positions: The second largest effect is a local change of the relative positions of the multiple lensed images and the creation of so called astrometric perturbations. These anomalies are related to a local change of the first derivative of the lensing potential. Therefore, they can only be produced by a gravitational perturbation and cannot be caused by micro-lensing. In the case of resolved sources, astrometric anomalies appear as perturbations to the surface brightness distribution of highly magnified arcs and Einstein rings, and are sometimes referred to as surface-brightness anomalies (see Fig. 3 for an example). The level of perturbations that can be detected using a surface-brightness anomaly is set by the quality of the data and structure of the source surface brightness distribution (see Sect. 7 and Despali et al. 2022). For example, a subhalo with a mass of $10^6 M_\odot$ will produce distortions on angular scales of a couple of milli-arcsecond.

Image time delay: The weakest effect is a change of the lensing potential itself. In the case of multiply imaged quasars with a flux-varying source, this phenomenon is observed as a perturbation to the time delay (see Chap. 7) between the multiple images (Keeton and

Moustakas 2009; Cyr-Racine et al. 2016; Gilman et al. 2020). Unlike flux-ratio anomalies, time-delay anomalies are not affected by dust extinction in the lens galaxy. However, they suffer from stellar micro-lensing which induces time-delay changes of the order of days (Tie and Kochanek 2018). Time-delay anomalies due to subhaloes are typically of the order of a fraction of a day. At present, this is smaller than the typical time-delay uncertainty (equal or larger than a day, e.g., Fassnacht et al. 2002). To be an effective probe of the nature of dark matter, time-delay anomalies require, therefore, sensitive measurements with a high observing cadence.

Image polarisation angle: The presence of a field of Axion-Like Particles (ALPs) and its interaction with photons leads to the so-called phenomenon of birefringence whereby the polarisation angle of a linearly polarised source is rotated. If the field oscillates over time, so does the change in the polarisation angle in a way that is related to the mass of the particles. Due to gravitational time delay, the multiple images of strongly lensed sources experience a different level of rotation, leading to differential birefringence, which can be used to probe the particle mass and its coupling with photons (Basu et al. 2021).

4 Lens Modelling

The process of constraining the properties of dark matter with strong gravitational lensing is best understood as a (hierarchical) Bayesian inference problem with the following unknowns: the intrinsic properties of the source $\vec{s}$, the parameters of the main lens(es) mass distribution $\vec{\eta}$, and the amount and properties of low-mass haloes or fuzzy dark matter granules $\vec{\eta}_{\rm pert}$. These have to be simultaneously inferred from the observed data $\vec{d}$ to which they are related in a statistical sense via the following posterior distribution:

$$P(\vec{s}, \vec{\eta}, \vec{\eta}_{\rm pert}|\vec{d}) = \frac{P(\vec{d}|\vec{s}, \vec{\eta}, \vec{\eta}_{\rm pert})\, P(\vec{s}, \vec{\eta}, \vec{\eta}_{\rm pert})}{P(\vec{d}|M)}\,. \tag{6}$$

In the numerator, the first term is the Likelihood function and the second is the prior on the parameters of the model M. The term in the denominator is the marginalised Likelihood (also known as Bayesian evidence). A detailed description of each ingredient is provided in the following sections. The equation above is an exact expression of the inference problem at hand, and it encodes how the different components are related to each other. However, depending on the modelling approach (see Sect. 4.4), one may not make direct use of this posterior probability and instead adopt simplifying assumptions to make the inference problem more tractable.

4.1 The Likelihood

The Likelihood function returns the probability of observing the data, given a choice of model. In the context of strongly lensed unresolved sources, the data $\vec{d}$ is the set of image fluxes and positions. For resolved sources, the data is the surface brightness distribution in each image pixel in optical observations and a set of visibilities for interferometric ones. In the case of radio polarised emission, the data is given by the visibilities of the coherency vector. In studies that combine multiple data-sets of the same lens system at different wavelengths, the data can be thought of as a concatenation of the different observations, which originate from the same lensing potential, but with a different surface brightness distribution

of the source. In many cases, the Likelihood function of a model image being correct given the data is well approximated by a Gaussian distribution with uncorrelated noise.[2]

4.2 The Source

Sources in gravitational lens systems can be of a large variety. In the following, we consider two idealised cases: sources that appear as unresolved and those that are instead resolved by the observations. OPtically faint AGN and QSOs are examples of sources that tend to be unresolved by most observations. Resolved sources include galaxies and radio jets.

Unresolved sources: Traditionally, for gravitationally lensed sources that appear unresolved, either a point or a Gaussian source is assumed. Free parameters of the model are therefore the source position and flux, and in the latter case also the source size. Assumptions on the source size and shape can introduce systematic errors in the dark matter inference that are discussed in more detail below.

Resolved sources: Typically, one of the following methods is used to describe the surface brightness distribution on the source plane: an analytical (e.g. a Sérsic) profile, a pixellated model, a basis function regression (e.g. starlets and shapelets) or a deep generative model. Here, we briefly discuss the main strengths and weaknesses of each approach.

The advantage of analytical models is that the number of free parameters is small, and the modelling procedure is fast. The main drawback is that such simplistic sources are an unlikely representation of lensed star-forming galaxies, which are often clumpy and irregular (e.g. Belokurov et al. 2009; Borsato et al. 2024; Dye et al. 2018; Ritondale et al. 2019b).

Pixellated sources have enough freedom to fit complicated light distributions well. However, as the lensing problem is poorely constrained, they require a regularising prior (e.g. Suyu et al. 2006; Birrer et al. 2015; Vernardos and Koopmans 2022; Galan et al. 2022). The choice of prior is non-trivial and may not necessarily be physically motivated. A possible solution is the introduction of hyper-priors (Rizzo et al. 2018; Vernardos and Koopmans 2022), which have the advantage of retaining the freedom of a pixellated source while imposing physically-meaningful constraints. Another limitation of free-form models is that they are challenging from a computational perspective, especially for high-resolution interferometric data (Hezaveh et al. 2016; Powell et al. 2021). One more aspect to consider is that these models require constructing a regular or adaptive grid on the source plane. We refer the reader to Tagore and Keeton (2014) and Nightingale and Dye (2015) for a detailed discussion of biases related to different choices of source discretisation and regularisation schemes.

Recently, machine learning techniques have been introduced to model the source galaxies (e.g. Chianese et al. 2020; Adam et al. 2022; Karchev et al. 2022). These approaches can overcome some of the above limitations. However, their performance is sensitive to the choice of training data. It is currently unclear how to generate large training samples of realistic lensed galaxies at high angular resolution. It is, for example, unlikely that nearby galaxies are a good description of the high-redshift population. Similarly, lensed and unlensed galaxies at the same redshift are not observed on the same angular scales. Holzschuh et al. (2022), have shown how generative models can be used to create arbitrarily large samples of source galaxies from hydrodynamical simulations. However, it is unclear how well these simulated galaxies represent the population of observed lensed sources. As for pixellated sources, deep learning techniques also suffer from biases related to the data discretisation.

[2]However, optical images may have correlated noise as a result of the pixel re-sampling using, for example, the drizzle image processing.

Independently of the chosen model, some level of degeneracy always exists between structures in the source and structures in the lensing potential. Therefore, any assumption on the source light has important consequences for the inference of dark matter with strong gravitational lensing. We provide a more detailed discussion of this issue in Sect. 5.

4.3 The Lensing Potential

In this article, we focus our attention on galaxy-scale lenses. While galaxy clusters could also provide constraints on small-scale fluctuations in the dark matter distribution, most studies so far have focused on smaller scale deflectors. This choice is related to the challenge of modelling the more complicated mass distribution of galaxy clusters with enough precision.

4.3.1 Main Lens

For galaxy scale lenses, the main deflector is typically a single galaxy, most commonly but not limited to a massive early-type. For many years, the most common parametrization for its mass density distribution was a single power law (SPL) or a singular isothermal (SIE) elliptical profile, plus external shear. This choice was motivated by the analysis of relatively large samples of lens galaxies (e.g. Koopmans et al. 2009; Barnabè et al. 2011). However, it is worth noting that no existing sample of strong lenses is representative of the actual distribution of observable lenses in the Universe. That is, the sample of lens systems used so far for dark matter studies (e.g. SLACS, BELLS and CLASS) have very specific selection functions. *Euclid*, on the other hand, is expected to identify a single homogeneous sample that is much closer to the underlying distribution found in nature - e.g. much smaller Einstein radii and lenses at larger redshift, on average (e.g. Sonnenfeld 2022).

An important question is the level of complexity in the mass distribution of lens galaxies and how it affects the constraints on dark matter. For example, deep Near-Infrared (NIR) observations have revealed the presence of a disk component in several lenses that were previously assumed to be purely elliptical. It was also shown that these disks have a non-negligible lensing effect and account for most of the observed flux ratio anomaly (Hsueh et al. 2016, 2017). Similarly, Spingola et al. (2018) and Powell et al. (2022) have shown with VLBI observations that an SPL is a good description of the lens mass distribution of MG J0751+2716 only down to scales of a few milli-arcseconds. Below these scales more complex angular and radial structures become important, and lens models that are smooth on milli-arcsecond scales are not able to fully reproduce the data. In light of these and other results (see Sect. 5), more recent analyses have included the effect of multipole mass moments, such as boxiness and diskiness, as well as that of nearby satellite galaxies. The degeneracy between different forms of complexity in the lensing potential (e.g. subhaloes versus disks or multipoles) is a source of systematic error in the inference of dark matter. We discuss this problem and possible solutions in Sect. 5.

4.3.2 Low-Mass Haloes

In the following, we refer to subhaloes and field haloes collectively as low-mass haloes. The parameters describing this population are: the number of objects, their masses, positions, redshifts and mass density profiles. Different assumptions regarding these quantities can be found in the literature. Here, we provide a description of those that are most frequently used.

Analytical: most commonly, low-mass haloes are modelled as spherical systems with a Pseudo-Jaffe (PJ, e.g. Dalal and Kochanek 2002) or a (truncated) NFW (e.g. Gilman et al. 2019; Hsueh et al. 2020) profile. The mass-concentration relation of the NFW depends on the dark matter properties and is either taken from numerical simulations (e.g. Gilman et al. 2019) or is a free parameter of the model (e.g. Gilman et al. 2020a). In fully forward models, the number of objects as a function of their redshift and mass are drawn from a Poisson distribution with an expectation value derived from the halo and subhalo mass functions. The latter are set by the dark matter model and are taken from numerical simulations (see Sect. 2). On each redshift plane, the projected positions of low-mass haloes are generally assumed to be uniformly distributed, as motivated by numerical simulations (Xu et al. 2015).

Pixellated: low-mass haloes are described as linear local corrections to the lensing potential (Koopmans 2005; Vegetti and Koopmans 2009). Individually detected objects are identified as positive convergence corrections of the otherwise smooth lens mass distribution. As for pixellated sources, a regularising prior for the potential corrections must be defined (e.g. Vernardos and Koopmans 2022). Due to its free-form nature, this approach does not make a priori assumptions on the number and mass density profile of the low-mass haloes. Typically, the connection to specific dark matter models is done a posteriori as described in Sect. 4.4.

Gaussian Random Field: low-mass haloes are represented by a Gaussian Random Field (GRF, e.g. Hezaveh et al. 2016; Diaz Rivero et al. 2018; Díaz Rivero et al. 2018; Chatterjee and Koopmans 2018; Cyr-Racine et al. 2019; Bayer et al. 2023a,b). The corresponding power-spectrum, which is by construction well represented by a power-law, then carries information on the low-mass haloes abundance, mass function and density profile. Hence, these quantities do not have to be assumed a priori. As the assumption of Gaussianity only holds for the very low mass haloes that appear in great number, the more rare and massive objects have to be individually detected and separately treated. The connection to the properties of dark matter is done a posteriori and in terms of the power-spectrum (see Sect. 4.4).

4.3.3 Fuzzy Dark Matter Granules and Subhaloes

In FDM cosmologies, the small-scale structure of galaxy-scale haloes and their subhalo populations are markedly different from their CDM or WDM analogues. The main difference is that the main dark matter halo exhibits wave intereference on $\sim$kpc scales due to the ultra-low mass of the dark matter particle; this gives rise to $\mathcal{O}(1)$ fluctuations in the halo density, which are commonly termed "granules". FDM haloes that are self-consistent with regard to the governing Schrödinger-Poisson equations can be obtained via numerical simulation (Schive et al. 2014b; May and Springel 2023) or direct construction of wave-function eigen-modes (Yavetz et al. 2022). However, for the practical purpose of gravitational lens modeling, a faster analytic prescription is often preferred. To this end, Chan et al. (2020) and Kawai et al. (2022) derive statistical properties of FDM granules that can be used to quickly generate perturbations to a smooth lensing potential, which are consistent with an FDM halo. Laroche et al. (2022) implement this approach by randomly placing a large population of Gaussian density profiles in the lens, while Powell et al. (2023) use a Fourier-space approach to achieve a similar result.

4.4 Modelling Approaches

4.4.1 Semi-Linear

Warren and Dye (2003) presented a lens modelling approach for the analysis of data with a resolved source in which the latter is pixellated (see Sect. 4.2). The most probable a poste-

riori (MAP) source and main lens parameters are inferred from the posterior probability in Eq. (6). In the case of quadratic prior distributions, the MAP source is obtained by solving a linear system (hence the term semi-linear - see Birrer et al. 2017; Galan et al. 2022, for examples of a semi-linear techinique with a basis function regression model for the source). The Bayesian evidence (denominator in Eq. (6)) is used to compare different models for the lensing potential and different choices of regularizations.

Koopmans (2005) introduced the so-called gravitational imaging technique for the detection of low-mass haloes with galaxy-galaxy lensing. In this approach, the source is pixellated and the low-mass haloes are described as linear, pixellated corrections to the analytical main lensing potential (see Sect. 4.3.2). The methodology was fully embedded in the framework of Bayesian statistics with an adaptive source by Vegetti and Koopmans (2009) and extended to the 3D (one frequency and two spatial dimensions) and interferometric domain respectively by Rizzo et al. (2018) and Powell et al. (2021). Recently, Vernardos and Koopmans (2022) have further extended the original method by Koopmans (2005) to include physically motivated priors. Due to the pixellated nature of the potential corrections, the gravitational imaging methodology does not require any assumption on the number, mass and position of low-mass haloes. Indeed, Vegetti and Koopmans (2009) have explicitly shown that more than one subhalo can be identified (provided that they have an effect on the lensed images), and Dhanasingham et al. (2022) have introduced a formalism to differentiate between subhaloes and field haloes based on the two-point function of the effective deflection angle field. Moreover, the potential corrections are not limited to capturing the effect of low-mass haloes. As shown by Barnabè et al. (2009), Ritondale et al. (2019a) and Galan et al. (2022) they can be used to identify components in the lensing potential that are not captured by the main parametric lens model. Indeed, the freedom allowed to the lensing potential is one of the main advantages of this approach as one can directly identify and differentiate different forms of complexity. One disadvantage is that the method is not fully forward, and two more steps are required to derive constraints on the properties of the dark matter: assessing the statistical relevance of detections and non-detections, and the interpretation of these in the context of theoretical predictions.

Detections: Vegetti et al. (2010), Vegetti et al. (2012) and Ritondale et al. (2019a) have introduced the following criteria to define the detection of a low-mass halo as statistically robust. (i) The mass and position of the pixellated convergence corrections have to be consistent with those inferred from an analytical description of the low-mass halo. The latter is inferred from the posterior distribution with a non-informative prior on the object mass and position, and a given choice of mass density profile. (ii) The model that includes low-mass haloes is preferred over the smooth one with a Bayes factor of at least 50. Under the assumption of statistical Gaussian errors, this difference in Bayesian evidence corresponds roughly to a $\geq$10-σ detection. While this may sound overly conservative, this choice is made due to the presence of unaccounted-for systematic errors that can result in false positives at lower significance levels (see Ritondale et al. 2019a, for a study on false positive detections).

Recently, this issue was more systematically quantified by Nightingale et al. (2022). We discuss their work in more detail in Sect. 5. It should be noted that false detections are not limited to this lens modelling approach. They are intrinsic to the general problem of detecting low-mass haloes with lensing and their degeneracy with other aspects of the lens inference problem. If anything, requiring that the free-form and the analytical model are consistent with each other can significantly mitigate some of these issues and reduce the incidence of false positives.

Non detections: Vegetti et al. (2014) and Ritondale et al. (2019a) quantify the statistical relevance of the non-detections using the so called sensitivity function. For each pixel on the

image plane the sensitivity function returns the lowest subhalo mass that could have been detected with a Bayes factor of 50. One of the main draw-backs of the sensitivity function is that, depending on the size of the data, it can be computationally expensive to evaluate. For each pixel on the image plane one has to calculate the Bayesian evidence of the model with a subhalo of a given mass. Hence marginalizing over redshift, number, mass and mass density profile could be practically unfeasible. O'Riordan et al. (2023) have recently shown that, in principle, one can successfully overcome these computational limitations by calculating the sensitivity function with machine-learning approaches. In Sect. 7 we will discuss in more detail what sets the sensitivity of a given data set to the presence of low-mass haloes of a given mass.

Dark matter constraints: From the sensitivity function, one can then interpret detections and non-detections within a given dark matter model. This is obtained by calculating the posterior probability of the dark matter particle mass assuming that the number of low-mass haloes has a Poisson distribution with expectation value given by the halo and subhalo mass function from that specific dark matter model (Vegetti et al. 2014, 2018; Ritondale et al. 2019a; Enzi et al. 2021).

Hezaveh et al. (2016) have introduced a new formalism in which the presence of subhaloes in the lens galaxy is modelled as a GRF (see Sect. 4.3.2). From the lensing observations, one constrains the power spectrum of projected density fluctuations, which amplitude and shape can then be a-posteriori compared to predictions from different dark matter models. The advantage of this approach is that no a priori assumption is made on the properties of the low-mass haloes as these can be inferred from the analysis itself. As should be the case, Diaz Rivero et al. (2018) have shown that the amplitude and shape of the power-spectrum are sensitive to the abundance, mass density profile, and concentration of subhaloes. The main disadvantage is that the assumption of a GRF only holds for the lowest-mass objects $M < 5 \times 10^7 M_\odot$ (Hezaveh et al. 2016). Hence, the larger ones have to be first individually identified and then explicitly included in the mass model. Moreover, in its current implementation, this approach does not allow one to identify other forms of complexity in the lens mass distribution (these are unlikely to be well described by a GRF), which then introduce a systematic bias on the dark matter inference (e.g. Bayer et al. 2023b).

4.4.2 ABC

Approximate Bayesian Computation (ABC, Rubin 1984; Diggle and Gratton 2018; Tavaré et al. 1997; Turner and Van Zandt 2012; Liepe et al. 2014) is an algorithm rooted in Bayesian statistics to circumvent the direct calculation of intractable Likelihood functions. As such, it enables inference analysis based on simulated data sets computed in a forward fashion. ABC methods follow a common general process: (i) emulate the data many times with different underlying target parameters as well as noise realizations; (ii) compress the difference between the simulation and the data in a set of summary statistics to provide a metric distance between the simulation and the data; (iii) accept the proposed simulations and their underlying parameters if the distance metric is within a certain threshold ϵ and (iv) the accepted samples can be interpreted as posterior distributions with the prior being the draws of the simulator. If the acceptance criteria converges to the identical matching of the simulation and data, $\epsilon \to 0$, the accepted sample is identical to the posterior from the exact Likelihood expression applied on the summary statistic.

An accurate ABC inference requires three main components. The first one is accurate simulations including all relevant aspects affecting the data (or more specifically the summary statistic). The second ingredient is a summary statistic that captures significant aspects

of the signal of interest. Finally, one needs a sufficient number of simulations such that a narrow acceptance criteria (small ϵ) can be chosen that leads to convergence and an accurate posterior prediction. One of the main advantages of an ABC approach is that, in contrast to some machine-learning-based methods (see Sect. 4.4.4 for more details), the summary statistic is explicit and is a means of understanding the impact of possible sources of systematic errors. However, the choice of summary statistic is arbitrary, potentially leading to a significant loss of information and constraining power. Specifically, the choice of summary statistic and level of data compression determine the number of simulations needed for the ABC process to converge, potentially resulting in a loss of computational efficiency relative to machine learning approaches.

In the context of inferring the properties of dark matter with strong gravitational lensing, Birrer et al. (2017) were the first to propose an ABC method. In particular, they made use of elaborate summary statistics including of a substructure scanning approach and the map of relative Likelihood (Sect. 4.1) values in the reconstruction with and without a substructure. This scanning mechanism was meant to filter signal and not absorb other spurious effects between the simulations and the data. The methodology was designed for strong gravitational lens systems with a resolved source, which was modelled with a basis function regression method in the form of shapelets. We refer the reader to Enzi et al. (2020), He et al. (2023), Bayer et al. (2023a) and Bayer et al. (2023b) for other examples of summary statistics commonly used when modelling strongly lensed galaxies. Gilman et al. (2018), Gilman et al. (2019) and Gilman et al. (2020b) have made use of an ABC approach to analyse the fluxes and positions of strongly lensed quasars. In this case, as the size of the data $\vec{d}$ was small, no compression was required and the summary statistics were set to the difference in the flux ratio of the multiple images between the simulation and the data.

As the ABC is a forward method, subhaloes and field haloes are typically described by analytical mass profiles and have properties statistically drawn as described in Sect. 4.3.2.

4.4.3 Trans-Dimensional

One of the challenges in constraining the properties of dark matter with strong gravitational lensing is that the number of low-mass haloes in any given lens system is unknown. As a consequence, the model describing the low-mass halo population and its properties needs to have a variable and a-priori unknown number of free parameters. An additional challenge is that most of the low-mass haloes will be at or below the detection limit. Brewer et al. (2016) and Daylan et al. (2018) have proposed the use of trans-dimensional Bayesian inference approaches (Green 1995, 2003) to overcome these problems.

These methods apply probabilistic cataloging to images of strongly lensed systems (Hogg and Lang 2010; Brewer et al. 2013, 2016; Daylan et al. 2017; Portillo et al. 2017) and output an ensemble of probability-weighted (sub-)halo catalogs providing a good fit to data. The prior distribution for the properties of the low-mass haloes is specified hierarchically, so that their mass function is a natural output of the method. Sampling of the posterior can be done with reversible jump Markov Chain Monte Carlo with differences in the explicit sampling methods, such as Diffusive Nested Sampling (DSN, Brewer et al. 2016) or PCAT (Daylan et al. 2018). One can also evaluate the marginal Likelihood of the model, including over the unknown number of low-mass haloes, and the source and lens properties. In most applications, both the source and the lens are described by analytical models. However, there is, in principle, no limitation to couple a trans-dimensional treatment of low-mass haloes with, for example, pixellated sources. As for Machine-Learning based techniques (see following section), the trans-dimensional approach has been applied so far only to simulated observations.

4.4.4 Machine Learning

In recent years, it has been shown that neural networks can efficiently estimate the parameters of strong lens models directly from observations (Hezaveh et al. 2017; Perreault Levasseur et al. 2017; Schuldt et al. 2021). Motivated by these results, a number of works have explored machine learning methods for identifying subhaloes in mock observations (Ostdiek et al. 2020; Yao-Yu Lin et al. 2020; Diaz Rivero and Dvorkin 2020). Others have shown that subhalo summary statistics can be directly estimated from mock observations (Brehmer et al. 2019; Alexander et al. 2020a,b; Varma et al. 2020; Alexander et al. 2021; Vattis et al. 2021; Ostdiek et al. 2022). However, these works do not provide any rigorous uncertainty estimates.

To address this issue, Brehmer et al. (2019) proposed an approach relying on Neural Ratio Estimators (NREs). NREs transform the problem of inferring the value of a continuous variable into a classification problem between two sets. Using this, it is possible to calculate the posterior of a parameter as the ratio of the Likelihood, multiplied by the prior, and the evidence. This allows for better uncertainty estimates. However, the approach of Brehmer et al. (2019) is extremely data-hungry, making its scaling to realistic data non-trivial. A number of variants of NREs have been proposed to solve this problem (Cranmer et al. 2020; Coogan et al. 2020; Montel et al. 2022).

Uncertainties on the subhalo population can also be obtained similarly to those of the macro-model as proposed by Perreault Levasseur et al. (2017). Wagner-Carena et al. (2023) showed that it is possible to infer the parameters of the subhalo mass function over a population of gravitational lenses, in a Bayesian hierarchical formalism. They trained a neural network that directly predicts a parameterized distribution approximating the posterior of the low-dimensional macro-model parameters and subhalo mass function normalization (see also Vernardos et al. 2020). One of the existing challenges is how to consistently incorporate realistic sources of biases (e.g. complex selection functions from lens-finding neural networks) in the inference process. A possible solution to this issue has been proposed by Legin et al. (2022).

Together, these works have shown that neural networks can extract low dimensional information about the density fields, that is, the parameters of the mass function or $m_{\rm WDM}$. The main limitation of these methods, however, is that they are only tractable for the inference of low-dimensional representations, implicitly marginalizing over all nuisance parameters that are not explicitly estimated. At first glance, implicit marginalization appears appealing because the marginal posterior of the dark matter model parameters is the desired outcome. However, it hinders reproducibility and confirmation of the results by alternative, more traditional approaches. Machine learning models do not predict, at least for now, the actual distribution of density in the foreground, or the surface brightness of the background source. One cannot therefore compare their predictions with the data by ray-tracing through the model favoured by the neural network.

If, for example, excess power is detected in the mass function, it would be challenging to identify the specific feature in the data that accounts for it. Investigating whether a neural network's preference for a given dark matter model comes from a massive subhalo or a population of low mass subhaloes would be intractable in most machine learning frameworks developed to date. The lack of explicit predictions of physical features like density or brightness distributions, makes it difficult to verify measurements of low-dimensional substructure statistics by neural networks using more traditional methods.

One of the central issues in modelling the physical features of strong gravitational lenses, either with traditional analysis methods or with deep learning, has been that of defining pri-

ors over such high dimensional spaces. Recent advances in denoising diffusion-based models are now making this previously-intractable problem possible (Song et al. 2020). Further, Adam et al. (2022) have shown that a neural network can learn the score of the prior over background source images, learned from unlensed high-resolution images of galaxies. By adding the Likelihood score to this learnt prior score and using a reverse-time stochastic differential equation solver, the authors can obtain samples from the posterior over background source pixels. Generalizing the framework of denoising score-based models to solve highly non-linear problems such as the reconstruction of density maps in strong gravitational lenses is an active area of research.

5 Degeneracies and Systematic Errors

When assessing the robustness of strong gravitational lensing constraints on dark matter it is important to consider the effect of degeneracies (intended here as a single degeneracy, represented by an n-dimensional subspace of the model parameters, and related to the inadequacy of the available data to constrain the model under consideration) and systematic errors. Some of these are related to the measurement at hand or unsolved theoretical questions and affect both unresolved and resolved sources. Others are lens modelling and data dependent. All of them are discussed in this section.

5.1 Degeneracy with Complex Macro-Models

For any analytical model of the main deflector, a degeneracy exists between the macro-model parameters (e.g. Einstein radius and external shear) and the presence and properties of low-mass haloes. Its strength depends on the data signal-to-noise ratio (SNR) and angular resolution, and the properties of the low-mass haloes themselves. For low-mass haloes that can be individually detected, the more concentrated their density profile and the closer to the lensed emission their position, the smaller the degeneracy with the lens properties (Despali et al. 2022).

At the same time, real galaxies are unlikely to be simple elliptical objects and are expected to have complex radial and angular structures (e.g. Spingola et al. 2018; Powell et al. 2022; Van de Vyvere et al. 2022). Unmodelled components in the lensing potential are likely to lead to an overestimation of the amount of low-mass haloes or FDM granules, resulting in a biased inference on the properties of dark matter. For example, Xu et al. (2015) have shown that the population of CDM subhaloes from the Aquarius (Springel et al. 2008) and Phoenix simulations (Gao et al. 2012) alone cannot reproduce the level of flux-ratio anomalies in eight strongly lensed quasars from the CLASS survey (Myers et al. 2003; Browne et al. 2003), under the assumption that those lenses are well represented by an SIE plus external shear model. As field haloes from the Millenium-II simulation (Springel et al. 2005) alleviate, but do not solve this discrepancy (Xu et al. 2012), they concluded that other forms of departure from a power-law macro-model may be contributing to the observed signal. Thanks to deep NIR observations of the CLASS gravitational lens systems B1555+375 and B0712+472, Hsueh et al. (2016) and Hsueh et al. (2017) were able to show that previously undetected stellar disks are responsible for most of the observed flux-ratio anomaly in these systems. Indeed, using mock simulated data, Gilman et al. (2017) and Hsueh et al. (2018) have reported that baryonic structures in the main lens can lead to an increase of the probability of large flux-ratio anomalies of between 10 and 20 per cent, depending on the lens galaxy morphology (see Fig. 4). Similarly, from the analysis of the Cosmic Horseshoe lens

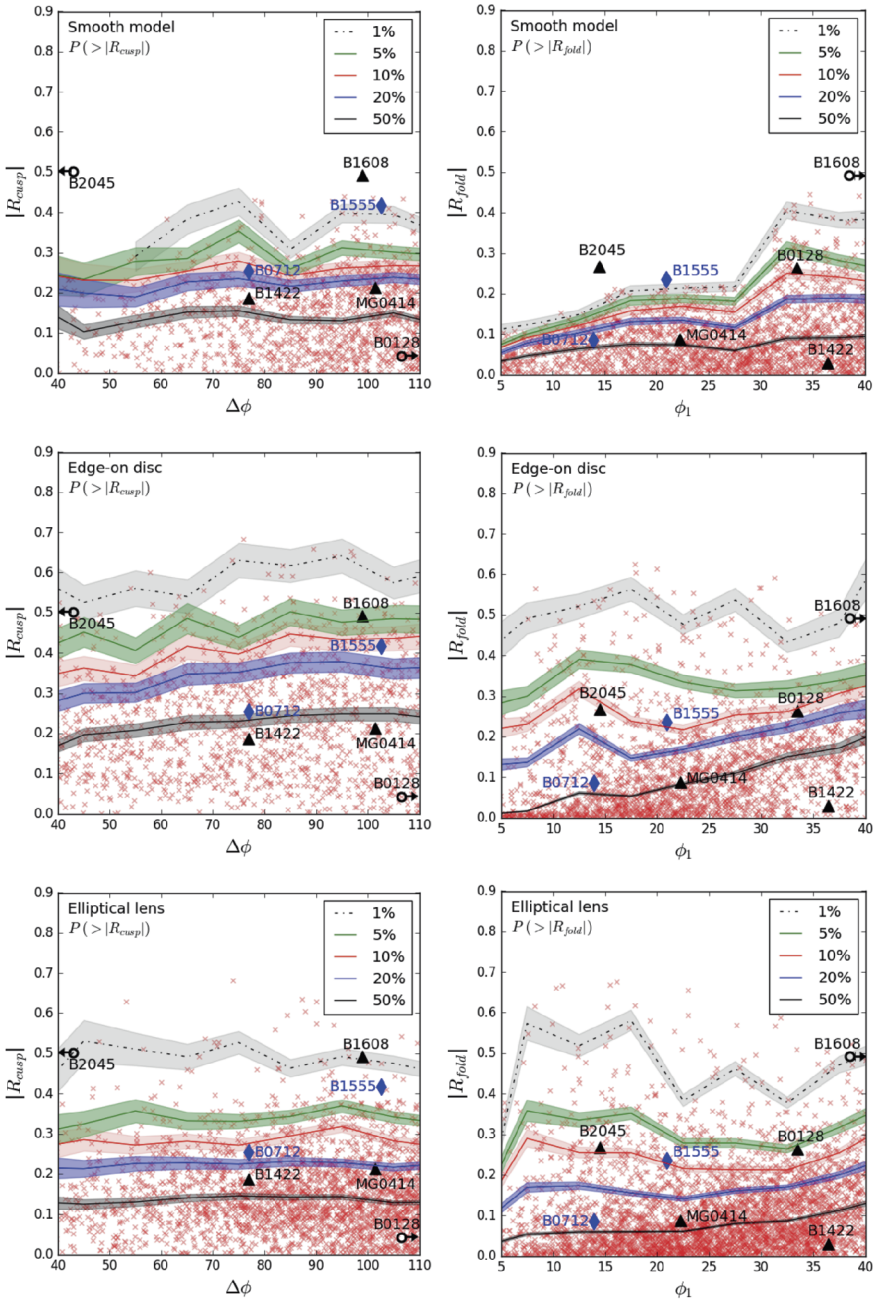

Fig. 4 Strength of the flux-ratio anomaly for a cusp (left) and fold (right) configuration arising from different mass distributions: an elliptical smooth power-law (top), an edge-on stellar disk (middle) and an early-type galaxy (bottom) selected from the Illustris simulation (Vogelsberger et al. 2014b). The strength of the anomaly is expressed in terms of the $|R_{\rm fold}|$ and $|R_{\rm cusp}|$ values, which are related to the observed flux-ratio anomalies via the equations (4) and (5), respectively. The curves represent 1, 5, 10, 20, and 50 per cent probabilities to find values of $|R_{\rm fold}|$ and $|R_{\rm cusp}|$ larger than a given value for fixed opening angles ϕ_1 (○) and $\Delta\phi$ (○). The panels are taken from Figs. 5, 6 and 7 in Hsueh et al. (2017)

system, Brewer et al. (2016) concluded that the inferred substructure population might have partially mimicked larger scale components not included in the primary lens model. He et al. (2023) have found that deviations from an elliptical shape that are not explicitly included in the macro-model lead to a biased characterisation of correctly identified subhaloes as well as false positive detections. Similarly, O'Riordan and Vegetti (2024) showed that multipole perturbations to the angular structure of the lensing galaxy are a significant source of false positive subhalo detections at larger masses. They concluded that these perturbations must be included in the model for detections to be reliable.

Nightingale et al. (2022) have performed a systematic study of the degeneracies between the macro-model and isolated subhaloes. From the analysis of a sample of fifty-four gravitationally lensed galaxies from the SLACS and BELLS GALLERY surveys (Bolton et al. 2008; Shu et al. 2016), they initially reported thirty-four subhalo detections at low significance. Upon further analysis, it is found that sixteen of these thirty-four are due to a degeneracy with the lens light (see Sect. 5.3) and five are due to insufficient source plane resolution. The remaining thirteen false positives are macro-model dependent with eight due to an overly simple lens mass model: a subhalo is favoured because it can replicate the effect of the missing complexity, instead when radial or angular structure in the lens is included, the addition of a subhalo is penalized by the Bayesian evidence. These false positives can be accounted for by including in the lens mass models more radial (e.g. the broken power-law model) and angular (e.g. multipoles) structure in two and six cases, respectively.

In general, the analysis by Nightingale et al. (2022) shows that more complicated mass distributions can both remove and add a subhalo candidate depending on the lens system and the type of model considered (e.g. multipoles versus composite mass distribution). As a consequence of this effect, results based on one lens system cannot be easily generalised to other objects. The situation is further confounded by the fact that the nature of the macro-model is unknown a priori and likely dependent on each lens galaxy formation history. While stellar disks may be visually identified with appropriate observations (Hsueh et al. 2016, 2017; Nierenberg et al. 2020), this is not necessarily the case for other forms of radial and angular structure. Moreover, depending on the spatial scales affected, the latter may be identified and characterized only with very-high angular-resolution data (Powell et al. 2022). These results highlight the importance of allowing for models other than a smooth SPL and modelling each lens in as much detail as the data will support, before proceeding with the detection of low-mass haloes.

While this degeneracy is intrinsic to the measurement itself and affects any type of lens modelling technique and data, it is particularly thorny for unresolved sources and models that solely rely on analytical macro-models.[3] In the first case, the data (at most, eight positions and four flux measurements) provide only limited information on the lens model. In the second case, for each lens system, one needs to marginalise over a wide range of macro-model assumptions. Resolved sources, where the potential is modelled with a free-form approach (Sect. 4.4) have in this respect an advantage: the data has more constraining power and the freedom allowed to the potential makes it possible to detect and potentially differentiate various mass components from each other (e.g. Galan et al. 2022).

In reality, the degeneracy between the lens macro-model and dark matter fluctuations, does not act in isolation. Its net effect is the result of its interplay with another degeneracy, that between the lensing potential and the source light distribution. We discuss the latter in the following section.

[3]These also include the case where low-mass haloes are described by a GRF, as the latter is an unlikely characterisation of (baryonic) structures in the lens mass distribution.

5.2 Degeneracy with the Source

5.2.1 Unresolved Sources

The angular size of the background source relative to that of a low-mass halo of a given mass sets the level of perturbation to the lensed images magnification. This effect introduces a degeneracy between the amount of low-mass haloes, micro-lensing by stars in the main deflector and the unknown size of the source. Micro-lensing by stars (see Chap. 5) becomes problematic when the image flux is gathered from a region surrounding the background quasar that is less than ~ 0.1 pc in diameter. It is responsible for an overestimation of the amount of low-mass haloes and hence a bias in favour of colder dark matter models. One can mitigate or even remove its effect with observations at wavelengths that are known to originate from an extended region around the source or by monitoring the system for a sufficiently large amount of time.

Provided that the source is large enough to avoid micro-lensing, uncertainties in the intrinsic size of the emission region translates into uncertainties in the amount of low-mass haloes. An overestimation (underestimation) of the former leads to an underestimation of the latter and a bias in favour of warmer (colder) dark matter models. Typically, one tries to account for this degeneracy by adopting observationally motivated priors (e.g. Koopmans et al. 2003; Chiba et al. 2005; Müller-Sánchez et al. 2011) and marginalising over the size of the source.

Another source of systematic error is related to flux variations in the emission region over time. Flux changes appear with a time delay between different positions on the image plane. As a result, single-epoch measurements sample the intrinsic light curve of the source at different times for the different lensed images. This effect leads to flux measurement errors that can be as large as 20 per cent (Dalal and Kochanek 2002; Koopmans et al. 2003).[4] It can be mitigated by monitoring and averaging the observed flux over a long period of time, or correcting for the time-delay.

At radio wavelengths, propagation effects, such as free-free absorption and scatter broadening can alter the measured properties of the different lensed images. As these effects have a strong wavelength dependence, they can be identified and corrected for with multi-wavelength observations (e.g. Winn et al. 2004; Biggs et al. 2003; Mittal et al. 2007).

5.2.2 Resolved Sources

The detection of low-mass haloes with resolved sources is based on the idea that the many pixels on the image plane provide redundant information about the source surface brightness distribution, allowing one to separate structures in the background object (which appear two or four times in the data) and structures in the lensing potential (which produce a relatively localised effect on the lensed images). In practice, however, due to the presence of noise in the data and the smoothing effect of the telescope point spread function, a degeneracy exists.

The extent of this degeneracy is strongly dependent on how the source and lensing potential are modelled. Vernardos and Koopmans (2022) have studied in detail the case of a

[4] It is possible for radio sources to show intrinsic variability of 10 per cent or more on the order of less than 100 days (Fassnacht et al. 2002). This may be because some of the emission is coming from much smaller regions, such as shocks in the jet. On the other hand, Koopmans and de Bruyn (2000) and Koopmans et al. (2003) detected changes to the fluxes of the individual lensed images of the order of 20 per cent. While they found these to be rare, at least some of them, were related to calibration issues, for others microlensing could also be an explanation..

pixellated source and potential corrections. They concluded that the two can partly absorb each other's complex structures in a way that depends on the form of the regularisation, the pixellatisation resolution and the actual complexity in the data (see also Bayer et al. 2023a). For example, when modelling a lens system, which is well described by a smooth analytical lens mass distribution and a complex source, the potential corrections can partly absorb fluctuations in the latter that are not well captured by the grid resolution and regularisation. Similarly, the source can adapt to compensate for the lack of structure in the model for the lensing potential. Interestingly, Vernardos and Koopmans (2022) find that the degeneracy between complexity in the source and in the potential mainly results in a biased lens macro-model and source, while the statistical properties of the potential corrections are well recovered. This suggests that, at least in the free-form approach, this degeneracy should not result in biased constraints on the properties of dark matter. However, a detailed investigation of this issue as a function of data type (e.g. optical or interferometric) and quality (e.g. angular resolution, signal-to-noise ratio and uv-coverage) is still lacking.

At the other end of the spectrum, models with analytical sources and potentials are likely to result in dark-matter constraints that are biased towards models that are colder or have a lower FDM particle mass. As the only complexity allowed in the analysis is in the form of low-mass haloes or FDM granules, these are then likely to absorb structures in the source as well as in the macro-model. Identifying suitable priors for the lensing potential and source light is therefore a key ingredient to infer the properties of dark matter with strong gravitational lensing.

5.3 Degeneracy with the Lens Light

Optical data includes light emission from the lens galaxy. This contribution is either pre-subtracted from the data (e.g. Vegetti et al. 2010) or inferred during the lens modelling analysis (e.g. Ritondale et al. 2019b,a) and sometimes used as an extra constraint on the lens mass distribution (e.g. Nightingale et al. 2022). Typically, it is described via a two dimensional B-spline function (e.g. Vegetti et al. 2014) or an analytical profile such as a (combination of) Sérsic model (e.g. Ritondale et al. 2019a; Nightingale et al. 2022). As for the lens mass distribution, simplistic models for the lens light may fail to reproduce complex radial and angular structures, as for example, boxy or disky isophotes and dust lanes. As a result, false positive detections of low-mass haloes may be obtained (Nightingale et al. 2022). It is therefore important to test candidate detections against different assumptions for the lens light (e.g. Vegetti et al. 2012; Nightingale et al. 2022) or, if possible, with observations at different frequencies.[5] For example, one can use observations in two or more wavelengths and the information carried by the multiple lensed images to correct for the effect of dust in the lens galaxy (e.g., Suyu et al. 2009).

5.4 Some Considerations on the Low-Mass Halo Density Profile

Low-mass haloes with a more concentrated mass density profile are more efficient lenses and are, therefore, more likely to be detected (e.g. Despali et al. 2018). This effect opens up the possibility of extracting further information on the properties of dark matter (e.g. Amorisco et al. 2022; Gilman et al. 2020a, 2021). At the same time, however, it introduces two related challenges in the interpretation of the observations within a given dark matter model. The first challenge is related to the robustness of the theoretical predictions and how they are

[5] Ideally at frequencies at which the lens does not emit any light.

affected by baryonic physics (Heinze et al. 2023) and the resolution of the simulations (see Sect. 5.6 for further discussions). The second one is related to the fact that the detected low-mass haloes are likely to be a biased sub-sample of the general population, an effect that needs to be taken into account in the inference process.

5.5 Some Considerations on Interferometric Data

At present, radio interferometetry (e.g. Smirnov 2011) provides the highest angular resolution available for strong gravitational lensing observations. In principle, this makes it, (for resolved sources), the most sensitive probe of the halo and subhalo mass functions, with very long baseline interferometry (VLBI) arrays capable of individual halo detections down to $10^6 M_\odot$ (McKean et al. 2015). However, modeling radio interferometric observations of strong gravitational lenses is challenging given the very large data sizes, and is an area of active research.

It is preferable to model radio interferometric observations directly in the native visibility space (a visibility is a Fourier component of the sky brightness as measured by two antennas at a given time and frequencey interval). In principle, it is possible to model a gravitational lens observation by first imaging the data using some established deconvolution technique (e.g. CLEAN, Högbom 1974; or maximum-entropy, Cornwell and Evans 1985), then applying standard lens modelling techniques to the deconvolved image. However, on the space of the CLEANed images, the noise is correlated and not well characterised, and the CLEANing process may introduce artefacts in the surface brightness distribution that mimic the effect of low-mass haloes. Source-plane deconvolution algorithms for radio observations of gravitational lenses (such as LensClean; Kochanek and Narayan 1992; Ellithorpe et al. 1996; Wucknitz 2004) were the first to be explored as a solution to this issue. Direct χ^2 fitting in the visibility plane was then applied by several authors (Bussmann et al. 2012, 2013; Hezaveh et al. 2013) to observations of lensed dusty star-forming galaxies (DSFGs) taken with the Sub-Millimetre Array (SMA) and the Atacama Large Millimetre Array (ALMA). A fully Bayesian treatment for fitting interferometric observations, which included prior information on the source surface brightness, was finally realized by Rybak et al. (2015) and Hezaveh et al. (2016).

Amplitude and phase calibration errors (e.g. Pearson and Readhead 1984) in interferometric data can potentially masquerade as false-positive detections of low-mass dark matter haloes. This was investigated using ALMA observations of the DSFG SDP.81 by Hezaveh et al. (2016), with a test of the data sensitivity to the subhalo detection both with and without a treatment for phase errors. Hezaveh et al. (2013) and Hezaveh et al. (2016) addressed this issue by including a single antenna-based phase correction as a free parameter in the lens modeling, self-consistently incorporating uncertainties due to this systematic effect into the model posterior. It is expected that the problem of calibration errors is less relevant for cm-wavelength VLBI observations as the atmosphere is more stable over time and the antenna receivers are more sensitive. Strongly lensed sources observed with VLBI are typically radio-bright jets containing both extended and compact features, which help to provide robust phase calibration solutions prior to the lens modeling step. This is in contrast to mm-wavelength observations of DSFGs, which feature rather diffuse, low-surface-brightness emission; in this case modeling phase errors as part of the lens modeling pipeline likely yields more robust calibration solutions than *a priori* self-calibration. While it is clear that residual phase calibration errors have an effect on the rate of false-positive detections and sensitivity to low-mass dark matter haloes, there is yet to be a systematic study of this effect.

The size of the data is important when it comes to modeling antenna phases directly; the ALMA observation to which this phase-correction model was applied contains a small enough number of visibilities (5×10^5 after some additional binning) that a standard linear-algebra solver framework could be applied to the source inversion step (Warren and Dye 2003; Suyu et al. 2006). For cm-wavelength VLBI data, for which averaging can introduce additional systematics that degrades sensitivity to low-mass dark haloes, an FFT-based iterative solver is required in order to be computationally tractable (Powell et al. 2021, 2022).

5.6 Theoretical Unknowns

5.6.1 Resolution, Halo and Subhalo Mass Functions

Theoretical predictions for the abundance and structure of CDM haloes and subhaloes initially came from analytical models, such as perturbation theory (Zel'dovich 1970), the Press-Schechter model (Press et al. 1992), the statistics of peaks in Gaussian random fields (Bardeen et al. 1986) and the excursion set approach (Bond et al. 1991; Sheth and Lemson 1999). Predictions from these theoretical models have then been compared to the results from N-body (i.e. dark-matter-only) numerical simulations. This comparison has led to precise fitting functions for the halo mass function that take into account the non-linear evolution of structure formation (Sheth et al. 2001; Giocoli et al. 2008; Tinker et al. 2008; Despali et al. 2016). Similarly, the functional form of the NFW profile (Navarro et al. 1996) reflects the expectations for the density profile of a dark-matter-dominated structure that forms via hierarchical accretion. CDM N-body simulations (i.e. without baryonic physics) created with different codes from the same initial conditions agree very well with each other: the impact of numerical effects and that of different (sub)halo identification methods have been widely studied and are well understood, resulting in (sub)halo mass functions in agreement within a few per cent (Knebe et al. 2011; Onions et al. 2012; Okabe et al. 2013).

However, some uncertainties remain. These are mainly related to the resolution limit of the numerical simulations and the consequent fact that analytical predictions have only been tested down to a finite scale. Numerical effects are especially problematic for the subhalo population. For example, the artificial disruption of subhaloes related to the limited spatial resolution of the simulations (Green and van den Bosch 2019; Green et al. 2021) can lead to an underestimation of the number of such objects on scales of the resolution limit of a factor of 10 to 20 per cent. Moreover, while the density profile of isolated haloes is well understood, subhaloes are affected by tidal disruption and stripping inside the main halo and thus show a larger variety of profiles (Sawala et al. 2017; Moliné et al. 2017), which are not all well described by the same functional form.

WDM N-body simulations, in which the power spectrum cutoff is resolved, are known to undergo artificial fragmentation in filaments producing spurious clumps that, close to the resolution limit, can outnumber real structures. One challenge is thus to correctly identify and remove them from the (sub)halo catalogues: this can be achieved by studying the shapes of the Lagrangian initial regions that correspond to the final structures, and eliminating those that are very elongated (Lovell et al. 2012). Alternatively, Stücker et al. (2020) have developed a method to smooth the density field using phase-sheet methods and a high-resolution force calculation, in order to completely circumvent the issue and avoid the formation of spurious subhaloes.

FDM theories predict differences in the subhalo population of a lens, with a suppression of the halo mass function at low masses due to the large de Broglie wavelength of the dark matter particle. Characterizing the low-mass halo population in FDM cosmologies

is an area of active research. Analytic approximations to the FDM halo mass function in FDM have been attempted (Marsh and Silk 2014; Kulkarni and Ostriker 2022), but at this time only mass functions obtained from numerical simulations (Schive et al. 2016; May and Springel 2023) have been applied in a lens modeling context (Laroche et al. 2022). The mass-concentration relation for FDM haloes is also highly uncertain; Laroche et al. (2022) modelled it using an extended Press-Schechter formalism (Schneider 2015) assuming some correspondence between the gravitational collapse time-scales of FDM and CDM haloes. Additionally, FDM haloes contain a characteristic soliton core that alters their density profiles (Schive et al. 2014b; Chan et al. 2022). An accurate model for subhaloes around a lens galaxy is important to consider for inferences based on flux-ratio anomalies of unresolved sources, as subhaloes and granules can produce similar observational signatures. However, for FDM particle masses lower than $\sim 5 \times 10^{-21}$ eV, subhaloes are too few and too diffuse to impart a small-scale signature on the observed source morphology, and can be absorbed into a sufficiently complex macro-model. This leaves the presence of granules as the main source of constraint on the particle mass.

5.6.2 The Effect of Baryons

In the past few years, numerical simulations, and especially those with a CDM cosmology, have made significant progress. Large-scale structure simulations are now able to reproduce realistic galaxy morphologies and the observed scaling relations (Vogelsberger et al. 2014b; Schaye et al. 2015; Pillepich et al. 2018; Dubois et al. 2021), reducing some of the tensions between CDM and observations (Brooks et al. 2013). Despite these successes, uncertainties, which may affect the interpretation of strong gravitational lensing studies within a given model, persist. Feedback processes, that cause a loss of baryonic mass, alter the total halo mass in a non-trivial way that depends on the halo mass and the galaxy formation model (Sawala et al. 2015; Despali and Vegetti 2017; Pillepich et al. 2018; Garrison-Kimmel et al. 2019). As a result, the number density of low-mass haloes ($10^7 M_\odot < M < 10^{10} M_\odot$) is suppressed in hydrodynamical simulations by a factor between 10 and 40 per cent. This suppression is smaller than the one seen in most WDM models in the same mass range, as the inclusion of baryons further suppresses the halo and subhalo mass function (Lovell et al. 2019; Despali and Vegetti 2017). However, due to the lack of hydrodynamical simulations with high-enough mass resolution, it is at present unclear how these mass functions are affected by the baryon and dark matter physics below the probed mass limit.

Baryonic physics also affects the inner mass density profile of galaxies in a way that depends on the feedback model (e.g. Mukherjee et al. 2021) and its interplay with the dark matter model. For example, Robertson et al. (2019), Despali et al. (2019) and Shen et al. (2022) have found that, in hydro-simulations with elastic SIDM, haloes have a larger variety of density profiles (with respect to the non-elastic SIDM case) and that the shape of haloes is much closer to the CDM hydrodynamical case, than initially inferred from dark-matter-only simulations. Mocz et al. (2019) studied the interplay between baryons and fuzzy dark matter, finding that the first stars can form in filamentary structures along the cosmic web, instead of only in the collapsed haloes. These results, could have interesting implication for the analysis of strong gravitational lens galaxies. However, the limited spatial resolution available in simulations at the scale of massive galaxies prevents us from a robust comparison between observations and simulations. For example, simulated galaxies display a central density core, which is large enough to produce strongly lensed image configurations that are not observed. While these uncertainties affect simulations in all dark models, they are currently more problematic for alternative non-CDM models. The vast majority of

simulations where dark matter is different from CDM does not include baryonic physics (Lovell et al. 2012; Vogelsberger et al. 2014a) and is not yet at the level of the CDM case, in terms of resolution, number of objects and volume (Adhikari et al. 2022). Moreover, even when baryons are included, the sub-grid physics processes that describe their behaviour often remain calibrated on CDM simulations. Hence, it is unclear whether non-CDM hydrodynamical simulations provide a correct description of the interplay between dark-matter and baryons. Obtaining large samples of numerical simulations with different galaxy formation and dark matter physics, as well as the volume and resolution required for a meaningful comparison with strong gravitational lensing observations is a fundamental step for future works.

6 Historical Perspective

6.1 Unresolved Sources

The use of strong gravitational lensing as a probe of dark matter was first proposed by Mao and Schneider (1998). They showed that anomalies in the flux ratios (i.e. ratios that deviated from those predicted by smooth mass models) of lensed quasars could be accounted for by subhaloes in the lens galaxy. In particular, they focused on the two and three brightest images in a fold and cusp configuration, respectively. For a smooth lens mass distribution, the fluxes of these lensed quasar images should satisfy the asymptotic relations in Eqs. (4) and (5). Discrepancies between the observed flux ratios and the generic predictions are therefore an indication of some type of small-scale structure in the mass distribution. Mao and Schneider (1998) also pointed out that flux-ratio anomalies observed in optical data could easily be due to micro-lensing by stars in the lensing galaxy. Focusing on radio observations was, therefore, a better way to investigate the presence of subhaloes. At these frequencies, the lensed emission had a large enough angular extent as to be insensitive to micro-lensing by stars (although see Koopmans and de Bruyn 2000). The paper investigated both compact mass distributions (globular clusters with masses of $\sim 10^6 M_\odot$) and smoother fluctuations such as spiral arms in the lensing galaxy.

Mao and Schneider (1998) thus truly set the stage for subsequent investigations of perturbations by dark matter haloes by: (1) considering perturbations by larger-scale structures than stars and, (2) pointing out that the observations had to be conducted using sources that had angular scales that were large compared to the Einstein radii of the stars in the lensing galaxy. This second requirement ruled out using emission from the accretion disks and broad-line regions associated with the lensed AGN, which are sensitive to micro-lensing. However, observations at radio or mid-IR wavelengths could be used to investigate dark matter since the regions in the background objects that produce emission at these wavelengths are large enough to be mostly unaffected by micro-lensing by stars in the lensing galaxy, but small enough to be sensitive to perturbation by relatively low-mass dark matter haloes. Unfortunately, it was difficult to obtain large samples at these wavelengths, since only $\sim$10 per cent of AGN are radio loud, and ground-based observations at mid-IR wavelengths are extraordinarily difficult due to thermal emission from the Earth's atmosphere. Thus, for many years the sample of lenses that were useful for dark matter investigations was on the order of 10 systems, primarily discovered in the MG (Bennett et al. 1986; Langston et al. 1990; Griffith et al. 1990, 1991), JVAS (Patnaik et al. 1992; Browne et al. 1998; Wilkinson et al. 1998), and CLASS (Myers et al. 2003; Browne et al. 2003) radio surveys. Initial investigations focused on individual lenses, particularly radio-loud four-image systems that strongly violated

the standard relationships for merging images (Fassnacht et al. 1999; Marlow et al. 1999; Trotter et al. 2000; Biggs et al. 2004), and included some work that incorporated numerical simulations to understand subhaloes (Bradač et al. 2002).

The seminal paper by Dalal and Kochanek (2002) was the first analysis of flux-ratio measurements in a statistically significant sample, with a goal of testing the ΛCDM model. They examined the flux ratios in a sample of seven lens systems and found broad consistency with CDM. Although this analysis had a high impact for many years, it did have several shortcomings in the context of current approaches to using flux-ratio statistics to draw inferences on the nature of dark matter. These include using CDM-only simulations, using fairly simple lens models, only considering subhaloes within the halo of the primary lensing galaxy while not including line-of-sight haloes, using PJ mass profiles for the subhaloes, and being restricted to using the somewhat uncertain flux-ratio measurements that were available at the time.

For nearly two decades following this analysis, no new lens systems that had high-sensitivity radio or mid-IR flux ratio measurements were discovered, so subsequent investigations had to focus on extending or improving the analysis rather than working with larger samples. One improvement came from a monitoring program to look for extrinsic variability in radio-loud lenses, which had the additional benefit of providing high-precision flux-ratio measurements after correcting for any time delays in the systems (Koopmans et al. 2003). Other work investigated astrometric shifts and parity dependence as methods for determining the abundance of subhaloes (Chen et al. 2007; Chen 2009).

Another major effort addressed the problem by conducting ray-tracing analyses through high-resolution numerical simulations, which allowed the inclusion of lower subhalo masses and, thus, more thoroughly to explore the lensing effects of dark-matter subhaloes and other possible perturbers (Mao et al. 2004; Xu et al. 2009, 2010; Richardson et al. 2022). These studies incorporated not only the number of anomalies in the observed radio lenses, but also how much the observed flux ratios deviated from the predictions of smooth mass models.

Interestingly, several of these studies found that CDM subhaloes were not sufficient to explain the observations fully (Xu et al. 2009, 2015), even when including line-of-sight haloes (Xu et al. 2012), suggesting that more complex macro models were needed. Earlier work had reached a related conclusion from simulated data, finding that an edge-on stellar disk could cause violations of the standard cusp relation for the lensed image magnifications (Bradač et al. 2004). Subsequent work discovered exactly this type of situation in observed lens systems. In some systems with the most extreme flux-ratio anomalies, high-resolution imaging from ground-based adaptive optics and HST data revealed edge-on disk components of the lensing galaxies. These additional baryonic components could explain the observed flux-ratio anomalies without needing to resort to either subhaloes or line-of-sight haloes (Hsueh et al. 2016, 2017). Further investigations used simulated galaxies to confirm the importance of baryonic structures in the lensing galaxies (Gilman et al. 2017; Hsueh et al. 2018).

In parallel with the work on extending and improving the analyses was an effort to increase the sample size of observed four-image lenses by pushing past the traditional radio and mid-IR observations that had provided the primary samples for the analyses above. In particular, Moustakas and Metcalf (2003) proposed a spectroscopic technique based on the differential magnification of several different emitting regions in the lensed quasar, i.e., the continuum, broad-line region, and narrow-line region (NLR). This approach allowed them to separate contributions from the smooth lens model, micro-lensing, and lensing by subhaloes. This method was applied to a single very low-redshift lens that was observed with an integral field unit (IFU) spectrograph, and seemed promising (Metcalf et al. 2004). It is difficult to apply this technique to higher redshift systems using the seeing-limited ground-based observations used in Metcalf et al. (2004), due to angular resolution issues. However,

a similar approach has been successful when using either ground-based adaptive optics IFUs (Nierenberg et al. 2014) or HST grism observations (Nierenberg et al. 2017). This technique has led to the first major increase in the sample size of four-image systems with measurements that are useful for flux-ratio investigations (Nierenberg et al. 2020).

6.2 Resolved Sources

Koopmans (2005) was the first to propose the use of galaxy-galaxy lensing observations to detect subhaloes within the lens using the semi-linear pixellated approach described in Sect. 4.4. A few years later, Vegetti and Koopmans (2009) extended the original idea to be fully embedded within the context of Bayesian statistics.

Then, Vegetti and Koopmans (2009) proposed a statistical framework for the interpretation of both detections and non detections within the context of specific theoretical predictions. They also showed how the achievable level of constraints on the subhalo mass function parameters is related to the number of lenses in the sample and the sensitivity of the data. Recently, Despali et al. (2022) have provided a detailed quantification of how the latter depends on the data properties. We discuss their findings and relative implications in Sect. 7.

Vegetti et al. (2010) and Vegetti et al. (2012) were the first one to apply the pixellated gravitational imaging technique to real data taken with the HST and Keck-AO. They reported a 16-σ and 12-σ detection of two individual subhaloes in the gravitational lens systems SDSSJ0946+1006 (also known as the double ring or the Jackpot) and B1938+666, respectively. These detections, obtained in a pixellated fashion, were then modelled with a PJ profile. From the latter, a total mass of $\sim 10^9 M_\odot$ and $\sim 10^8 M_\odot$ was inferred for each system, respectively. Both detections have been independently confirmed (Minor et al. 2021; Sengül et al. 2022). However, Despali et al. (2018) and Sengül et al. (2022) have found that the detection in the system B1938+666 is more likely a field halo. Whether the concentration of these two objects is consistent with CDM predictions is currently under investigation (e.g. Minor et al. 2021; Şengül and Dvorkin 2022). From the analysis of the ALMA long baseline campaign data for the lens system SDP.81, Hezaveh et al. (2016) reported the detection at the 5-σ level of a subhalo with a total PJ mass of $\sim 10^9 M_\odot$. Inoue et al. (2016) also found a detection in this lens system. However, the inferred subhalo position and lens macro-model are inconsistent between the two analyses. Further investigations are required to understand the origin of this discrepancy.

Focusing, for the first time, on a larger number of strong gravitational lens systems, Vegetti et al. (2014) found no additional subhaloes in a sample of ten SLACS lenses, in the mass regime probed by the data. Recently, Nightingale et al. (2022) have searched for the presence of subhaloes in fifty-four lens systems (the largest number considered so far) from the SLACS and BELLS gallery samples. They reported two candidate detections, one of which matches the one by Vegetti et al. (2010) in the Jackpot lens.

While early studies considered the subhalo population only, Li et al. (2017), Despali et al. (2018) and Amorisco et al. (2022) have shown the contribution from field haloes to be important and in some cases dominant. This is a significant result. Unlike for subhaloes the properties and number of field haloes are better understood from a theoretical perspective (see Sect. 5.6), and the resulting increase in the number of detectable objects per lens allows for stronger constraints on dark matter with fewer systems. Allowing for the contributions of both populations, Ritondale et al. (2019a) concluded that their lack of detection in twenty-one lens systems from the HST BELLS gallery sample is consistent with the CDM model.

Dark-matter constraints from strongly lensed resolved sources have been mainly limited by the amount of available data with enough angular resolution. In recent years, efforts have

been made to increase the number of known strong gravitational lens systems (e.g. Lanusse et al. 2018; Huang et al. 2021; Petrillo et al. 2019; Cañameras et al. 2021; Rezaei et al. 2022), as well as the number of observations with improved angular resolution with, for example, Keck-AO (Lagattuta et al. 2012) in the NIR, ALMA in the sub-mm (Spilker et al. 2016) and VLBI at cm-wavelenght (Spingola et al. 2019). At same time, several new lens modelling approaches have been developed (see Sect. 4.4 and references therein).

Existing data-sets as well as simulated ones, have been used to improve our knowledge of systematic errors and degeneracies (see Sect. 5 and references therein), and our understanding of the signal under study. For example, Amorisco et al. (2022) showed that an improvement on the level of dark matter constraints can be obtained by taking into account the low-mass haloes mass-concentration relation (and how it changes with the dark-matter model) and its scatter. Similarly, ray-tracing through numerical simulations has been instrumental to quantify the lensing effect arising from smaller- and larger-scale structures (e.g. Enzi et al. 2020; He et al. 2023) in different dark matter models (Despali et al. 2019, 2020).

7 Dark Matter Constraints

7.1 Unresolved Sources

Since 2019, four new analyses (Hsueh et al. 2020; Gilman et al. 2020b,a; Laroche et al. 2022) have characterized the properties of low-mass haloes using a sample of quadruply-imaged quasars. These works interpret strong lensing data in the context of a variety of scenarios, including classes of dark matter such as warm dark matter, ultra-light dark matter, and self-interacting dark matter, as well as early Universe physics that alters the power spectrum of primordial density fluctuations.

Hsueh et al. (2020) and Gilman et al. (2020b) analyzed a sample of strong lens systems in the context of warm dark matter. Their inference places an upper limit on the free-streaming length of dark matter equivalent to that of a 5 to 6 keV thermal relic dark matter particle, and constrains a variety of sterile neutrino models with varying production mechanisms (Zelko et al. 2022). Gilman et al. (2020a) used the sensitivity of the relative magnifications among the lensed images to infer the concentrations of CDM haloes, an analysis that was later generalized by Gilman et al. (2022) to make a direct connection between the abundance and internal structure of dark matter haloes and the primordial matter power spectrum on small scales $\left(k > 10\,\mathrm{Mpc}^{-1}\right)$. The resulting inference on the concentration-mass relation and power spectrum agreed with the CDM prediction. Laroche et al. (2022) interpreted the same sample of eleven four-image lenses as analysed by Gilman et al. (2022) in the context of ultra-light dark matter, showing that the granular structure of the host halo density profile that arises from quantum wave interference effects can impact image flux ratios in a similar manner to dark matter haloes. Finally, building on work by Gilman et al. (2021), Gilman et al. (2022) interpreted the same sample of eleven lenses in the context of self-interacting dark matter and showed that existing data disfavors SIDM models with large amplitudes at low speeds, such as those that can arise from resonances in the self-interaction cross section, assuming the large amplitude of self-interaction cross section drives low-mass haloes to core-collapse. By combining observations of the Milky Way satellites with the sample of strongly lensed unresolved sourses from Gilman et al. (2022), Nadler et al. (2021) have derived a limit on the half-mode mass of $M_{\mathrm{hm}} < 10^7 M_{\odot}$ (i.e., $m_{\mathrm{WDM}} > 9.7$ keV) at the 95 per cent confidence level (see Fig. 5).

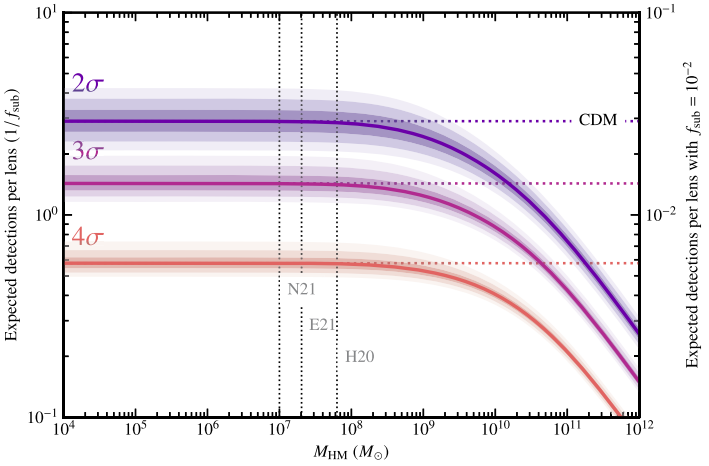

Fig. 5 Expected number of subhaloes per lens as a function of the half-mode mass from Euclid-like observations. Each curve (with 64 per cent, 95 per cent, and 99 per cent confidence areas) is for a different level of significance of subhalo detection. The horizontal dotted lines display the expected number of detectable subhaloes in CDM (see O'Riordan et al. 2023, for more details). The vertical dotted lines show the current 95 per cent upper limits on the half-mode mass from Nadler et al. (2021) and Hsueh et al. (2020) together with the 1/20th of the maximum Likelihood from Enzi et al. (2021)

These analyses have incorporated the latest theoretical understanding of structure formation in CDM and alternative dark matter models, such as the halo mass function and concentation-mass relation in warm dark matter, the process of core-collapse that is expected to occur in self-interacting dark matter, and the phenomenon of wave-interference unique to ultra-light dark matter. At the same time, Basu et al. (2021) have introduced a novel approach to constrain Axion-Like Particles dark matter models from the differential birefringence effect imparted on the strongly lensed images. Using broad-band polarisation observations of the lens system B1152+199 from the Karl G. Jansky Very Large Array (VLA), they derived an upper bound on the ALP-photon coupling between $g_{a\gamma} \leq 9.2 \times 10^{-11}$ and 7.7×10^{-8} eV at the 95 per cent confidence limit for an ALP mass between $m_a = 3.6 \times 10^{-21}$ eV and 4.6×10^{-18} eV.

Two recent innovations have expanded the scope of strong lensing of unresolved sources as a probe of fundamental dark matter physics. First, the sample size of lenses suitable for a subhalo inference doubled with measurements of relative image fluxes from narrow-line emission around the background quasar. Nuclear narrow-line emission, which emanates from an area in the source plane with a typical size between 10 to 100 pc, subtends angular scales on the sky much larger than a micro-arcsecond. This renders the relative brightness of lensed images immune to micro-lensing, while retaining sensitivity to milli-lensing by dark matter haloes. Second, open-source software to model gravitational lens systems and to generate populations of dark matter haloes for lensing computations have enabled ray-tracing simulations to be performed in parallel on computing clusters with realistic background sources and full populations of subhaloes. At the same time, recent analyses (from 2021 onwards) have made some efforts to mitigate potential systematic uncertainties associated with the lens macro-model by including the contribution of multipole mass moments.

7.2 Resolved Sources

Most studies based on resolved lensed sources are so far consistent with the CDM model. For example, Vegetti et al. (2014) and Hezaveh et al. (2016) have inferred a dark matter fraction in subhaloes (i.e. the normalisation of the subhalo mass function) that is consistent with the subhalo population in CDM simulations (Springel et al. 2008; Xu et al. 2015; Despali and Vegetti 2017). From an analysis (which only include the contribution of subhaloes) of the lens system RXJ1131−1231, Birrer et al. (2017) have derived a 2-σ lower limit on the particle of a thermal relic dark matter model of $m_{\rm th} > 2$ keV. On the other hand, Bayer et al. (2023b) have found an upper limit on the power-spectrum of mass density fluctuations in the lens system SDSS J0252+0039 that exceeds the value expected from CDM. Their result is likely driven by their choice of macro-model (SPL) and the lack of other form complexity beyond subhaloes.

Allowing for the contribution of field haloes, Vegetti et al. (2018) have derived constraints on sterile neutrinos that show a preference for colder dark matter models: $\log M_{\rm hm}[M_\odot] < 12.0$ at the 2-σ level. This result excludes sterile neutrino models with neutrino masses $m_{\rm s} < 0.8$ keV at any value of the lepton asymmetry L_6. Ritondale et al. (2019a) reported zero detection of low-mass haloes in a sample of twenty-one strong gravitational lens systems from the BELLS survery, in agreement with CDM given the quality of the data. Recently, Enzi et al. (2021) have derived constraints on thermal relic and sterile neutrino dark matter models by combining the lensing results by Vegetti et al. (2018) and Ritondale et al. (2019a) with observations of the Lyman-α forest and the Milky Way satellite galaxies. They derived a joint limit on the thermal relic mass of $m_{\rm th} > 6.048$ keV (i.e. $M_{\rm hm} < 3 \times 10^7 M_\odot h^{-1}$) at the 95 per cent confidence level (see Fig. 5). This result is mainly set by the Milky Way and the Lyman-α forest. The lensing measurements alone lead to a 95 per cent confidence level lower limit of $m_{\rm th} > 0.6$ keV and $m_{\rm th} > 0.1$ keV, for the SLACS and BELLS samples, respectively.

While most published analyses of resolved sources show a preference for CDM, they do not rule out alternative and still viable dark matter models yet. This lack of constraints is partly due to the low number of lens systems available and the relatively limited quality of the data: signal-to-noise ratio and in particular angular resolution. Using realistic mock observations of varying data quality, Despali et al. (2022) have recently quantified how the sensitivity to subhaloes depends on the properties of the lens system (e.g. source structure and position relative to the caustics) and the data (i.e. signal-to-noise ratio and angular resolution). They concluded that the lowest detectable subhalo mass decreases linearly with signal-to-noise ratio, and more strongly with the angular resolution. An increase in the latter by a factor of two leads on average to an increase in mass sensitivity of a similar factor (for a fixed signal-to-noise ratio, lensing configuration and source properties). For example, existing HST observations ($< \mathrm{SNR} > \sim 3.5$ and $\mathrm{PSF_{FWHM}} = 0.09$ mas) have a maximum sensitivity of $M_{\rm vir}^{\rm NFW} = 10^9 M_\odot$, leading to an expected number of detectable subhaloes per lens in CDM consistent with the current number of objects detected so far (Vegetti et al. 2014; Ritondale et al. 2019a; Nightingale et al. 2022). These effects also explain why the constraints are, at present, less stringent (though possibly more robust) than those obtained with unresolved sources: predictions from different dark matter models mostly differ at halo masses smaller than currently probed.

Observations at very high-angular resolution are therefore key to probe the nature of dark matter with resolved sources. For example, from observations of the gravitational lens system MG J0751+2716 taken with the Global Very Long Baseline Interferometry array, Powell et al. (2023) have ruled out scalar FDM models with a particle mass $m_\chi \leq 4.4 \times 10^{-21}$

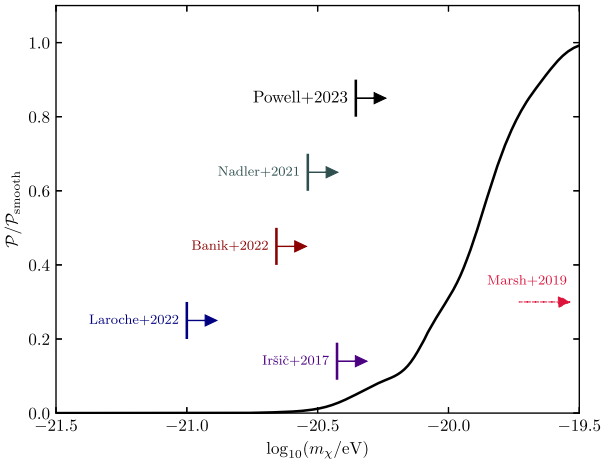

Fig. 6 Bounds on the FDM particle mass from different observational probes. The solid black curve and arrow show the fully marginalized posterior odds ratio and relative lower bound from Powell et al. (2023), respectively. These were derived from the analysis of mas-resolution observations of the lens system MG J0751+2716 taken with the Global Very Long Baseline Interferometry array. The results by Laroche et al. (2022, blue arrow) were obtained from a sample of eleven strongly lensed QSOs. Also shown are the constraints from the Lyman-α forest (Iršič et al. 2017, purple arrow), the Milky Way satellites (Nadler et al. 2021, green arrow), stellar streams in the Milky Way (Banik et al. 2021, dark red arrow). The limit by Marsh and Niemeyer (2019, red dashed arrow) lie beyond the limit of the plot, and were derived from observations of star clusters within the Milky Way Ultra-faint Dwarf satellite galaxy Eridanus II

eV. Their constraints, which were obtained from a single lens system with milli-arcsecond angular resolution, are more stringent than previously published results from larger samples of lensed quasars (see Fig. 6). Their work, together with the results by Despali et al. (2022) and O'Riordan et al. (2023), clearly demonstrates how a smaller number of high-angular resolution observations can be more effective at constraining the properties of dark matter than many lens systems with lower quality data. We will discuss this further in the context of future surveys in the following section.

8 Future Prospects

At present, the level of constraints that can be obtained on the properties of dark matter from both resolved and unresolved sources has mainly been limited by the amount of available data. Strong gravitational lensing is a rare phenomenon and the number of known systems with suitable data (e.g. high enough signal-to-noise ratio and angular resolution for resolved sources and the right frequency coverage for unresolved sources) is small (of the order of a few tens).

Thanks to ongoing wide-sky surveys the number of known strong gravitational lens system has significantly increased in recent years (e.g. Storfer et al. 2022). With the advent of the next generation of sky surveys with, e.g., Euclid, the Low-Frequency Array (LOFAR), the Square Kilometre Array (SKA) and the Vera Rubin Observatory, this number is expected to increase even further (e.g. Oguri and Marshall 2010; McKean et al. 2015). The size of these samples is unprecedented. Coupled with follow-up observations they will provide robust and meaningful constraints on dark matter.

8.1 Unresolved Sources

Increasing the sample size for four-image systems will reduce the statistical uncertainties of measurements made with these types of system. Provided that all sources of systematic error can be accounted for, this increased constraining power can lead to stronger constraints over various dark matter models, such as warm and self-interacting dark matter (Gilman et al. 2019, 2021; Hsueh et al. 2020). The existing analysis techniques applied to interpret data from multiply-imaged quasars can scale to match the increased sample size. Thus, computational costs will not limit the scientific output achievable with forthcoming data.

Follow-up observations will be required to precisely measure the positions and relative magnifications among the unresolved images of the lensed source. These observations can be performed with spaced-based observatories, such as HST and JWST (while they remain operational), but most likely with ground-based facilities with adaptive optics for optical and infrared-bright quasars (Nierenberg et al. 2014), and with the Very Large Array (VLA), the enhanced Multi Element Remotely Linked Interferometer Network (e-MERLIN) and VLBI for unresolved lensed radio sources. Upcoming observational facilities, such as the Keck All sky Precision Adaptive optics program (Wizinowich et al. 2022) and thirty-metre class telescopes, like the European Extremely Large Telescope (ELT), will provide exquisite astrometry and sensitivity with which to measure the relative image fluxes and positions. Likewise, the SKA will provide high resolution imaging at a resolution of 30 to 70 mas, which, when combined with VLBI, can provide astrometric measurements at sub-mas-arcsecond precision (e.g. Spingola and Barnacka 2020).

The JWST will soon deliver precise measurements of relative image fluxes in the mid-infrared at >20 μm (Nierenberg et al. 2021), emission that emanates from a more compact region (1 to 10 pc) around the background source than the nuclear narrow-line emission (10 to 100 pc) that has been measured with the HST and Keck-AO (Nierenberg et al. 2020). The spatial extent of the mid-IR emission renders these data immune to stellar micro-lensing and variability of the background quasar, systematic effects that one could conflate with the perturbation by low-mass haloes .[6] The more compact mid-IR emission that is measurable with the JWST increases sensitivity to perturbations by low-mass haloes relative to existing data because the minimum deflection angle that can affect the data scales with the angular size of the lensed source (Dobler and Keeton 2006). Mid-IR flux ratios measured with the JWST have anticipated sensitivity to populations of haloes less massive than 10^7 $M_\odot$ (Nierenberg et al. 2021). Moreover, the compact background sources measurable with JWST will increase sensitivity to the internal structure of low-mass haloes. This improved sensitivity, in combination with the expanded sample size of strong lens systems, will enable searches for populations of core-collapsed haloes, such as structures with logarithmic central density profile slopes steeper than -2 (Balberg et al. 2002; Turner et al. 2021). If detected, the existence of these objects would suggest dark matter has a velocity-dependent cross section with strong self-interactions at low speeds that triggers core collapse (Gilman et al. 2021; Turner et al. 2021; Yang et al. 2023; Gilman et al. 2022). Increased sensitivity to the internal structure of low-mass haloes will also enable stronger constraints on the concentration-mass relation of low-mass haloes (Gilman et al. 2020a). This type of measurement can be interpreted in the context of the primordial matter power spectrum on scales $k > 10$ Mpc^{-1} (Zentner and Bullock 2003; Gilman et al. 2022). However, as the background sources will

[6] Scattering of light into our field of view by the spatially-extended nuclear narrow-line and mid-IR emission regions acts as a low-pass filter that washes out variability in the quasar light curves on timescales less than the light crossing time.

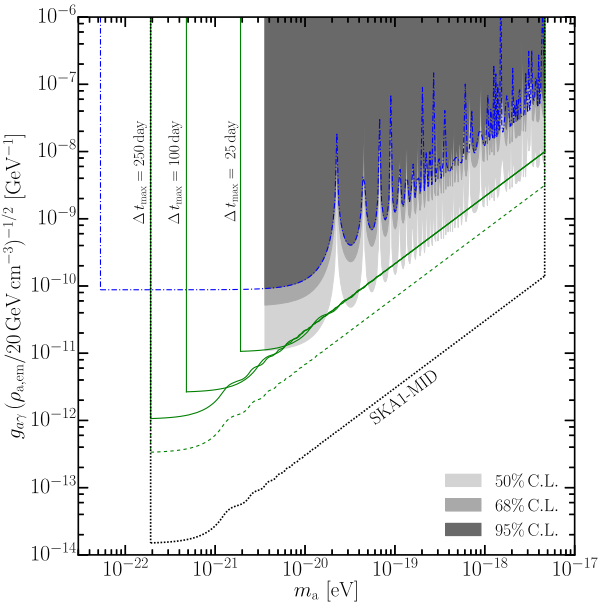

Fig. 7 Limits on the ALP-photon coupling from strong gravitational lensing. The dashed area shows current bounds from the gravitational lens system B1152+199. The dash-dotted blue line shows the expected constraint that can be obtained from monitoring B1152+199 over the course of ~ 5 year. The solid and dashed green lines show the predicted bounds for a sample of 100 and 1000 gravitational lens systems for different values of the maximum time delay ($\Delta\, t_{\mathrm{max}}$) on the observed plane. The dotted black line shows the parameter space that can be probed with the SKA. The figure is taken from Basu et al. (2021)

remain unresolved, their unknown surface brightness distribution will still stand as a potential source of systematic error. Moreover, in those cases without any extended emission from the quasar-host galaxy, the limited number of observational constraints provided by the data may lead to a potential systematic error in the macro-model.

At radio wavelengths (between around 4 and 18 GHz), large fractional bandwidths with, for example, the ngVLA and the SKA, will detect the emission from pc-scale radio sources, which are expected to be immune from micro-lensing (but see, e.g., Koopmans and de Bruyn 2000; Biggs 2023). The orders of magnitude improvement in sensitivity will allow monitoring of the lensed radio sources for cosmology (in the case of any intrinsic variability) or for dark-matter studies, when the radio source is found not to vary. While the large fractional bandwidths will allow radio propagation effects, such as free-free absorption or scattering, to be identified, which can either corrected for or used to create samples of lensed radio sources that do not show such issues. However, the main contribution that radio-selected samples can provide is our ability to characterise the source structure on mas-scales through observations with VLBI (e.g McKean et al. 2007; Spingola and Barnacka 2020). In general, it is worth noting that combining the data from multiple emission regions (mid-IR-bright torus, NRL, radio-jets) will allow various systematics associated with the source model to be quantified and possibly corrected for. This may include better constraints to the macro-model via large scale source properties, such as the optical/infrared emission from the stellar component of the quasar host galaxy or through high resolution imaging of the kpc-scale dust emission with ALMA (e.g. Stacey et al. 2021).

Finally, high-sensitivity observations with the LOFAR2.0 and SKA-MID of large samples of polarised and strongly lensed sources are expected to improve upon current bounds on the ALP-photon coupling by one to two orders of magnitude, depending on the ALP mass range (see Basu et al. 2021, and Fig. 7). Providing, thereby, competitive constraints on dark-matter models made of ALPs.

8.2 Resolved Sources

The larger number of strong gravitational lens systems with a resolved source that will be discovered by wide-sky surveys will represent a unique opportunity. However, follow-up observations at high angular resolution will be necessary to obtain meaningful constraints on the properties of dark matter. Recently, O'Riordan et al. (2023) calculated the sensitivity function for 16000 Euclid-VIS-like mock observations (see Fig. 5). They found most of the lenses in the sample to be completely insensitive to the presence of subhaloes with a mass lower than $M_{\rm max}^{\rm NFW} = 10^{11} M_\odot$. The most sensitive pixels yield a lowest detectable mass of $M_{\rm max}^{\rm NFW} = 10^{8.8 \pm 0.2} M_\odot$. Assuming CDM and a dark matter fraction in subhaloes of 0.01, this sensitivity leads to one detectable object in every seventy lenses. These results are in line with Despali et al. (2022) and the current number of detected objects (see previous section). Hence, Euclid will allow one to detect a number of subhaloes that is significantly larger than what has been possible so far, and potentially deliver tighter constraints on the amount of dark matter in subhaloes (i.e. the normalisation of the subhalo mass function) than currently possible. However, most of these objects will be relatively massive, and will probe (thermal relic) dark matter models with a half-mode mass of $M_{\rm hm} > 10^8 M_\odot$. These models have already been ruled out by other observations, including strongly lensed quasars. Similarly, if not slightly worse results are expected from the Vera Rubin Observatory, given its slightly worse angular resolution.

While the sensitivity to the presence of low-mass haloes increases linearly with decreasing signal-to-noise ratio, the angular resolution of the observation sets a hard limit on the lowest detectable halo and the spatial scales on which the dark matter distribution can be probed (Despali et al. 2022; O'Riordan et al. 2023). For this reason, follow-up observations with Keck-AO, HST and ALMA are likely to lead to an increase in sensitivity (relatively to Euclid) between two to three orders in magnitude in halo mass. With an angular resolution of a few milli-arcseconds, Global VLBI observations at 1.6 to 15 GHz, will allow one to detect masses as low as $10^6 M_\odot$ (McKean et al. 2015), and probe the general spatial distribution of dark matter on sub-kpc scales (e.g. Powell et al. 2023). Moreover, searches for milli-arcsecond scale separation images with VLBI will potentially reveal the presence of super-critical low-mass haloes, which existence is predicted by certain SIDM models (Casadio et al. 2021; Loudas et al. 2022). In the future, 30-metre class optical telescopes such as the ELT are likely to provide a similar level of sensitivity, while interferometric observations in the 10 to 100 GHz range with SKA-VLBI or the ngVLA will lead to an even stronger increase. This significant improvement in data quality will also result in better constraints on the properties of the lens macro-model. This effect will significantly reduce the role of one of the main sources of systematic uncertainty and will potentially have interesting implications for other scientific applications of strong gravitational lensing. A relatively small number of high-resolution observations is, therefore, expected to potentially deliver stronger constraints on the properties of dark matter than the several orders of magnitude larger sample of Euclid and Vera Rubin lenses. Note, however, that these facilities and also LOFAR and the SKA will be vital for finding the lenses needed for high-resolution follow-up observations.

9 Summary and Conclusions

Strong gravitational lensing provides a unique channel to constrain the dark matter distribution on subgalactic scales, and hence provide a key test of several dark matter models. In

this article, we described the process of inferring the properties of dark matter from strong lensing observations in terms of a Bayesian inference problem, and showed how it can be approached from different perspectives (Sect. 4). For each possible prior choice and lens modelling technique, we then discussed their advantages and limitations (Sect. 4.4). In Sect. 5 we provided an extensive discussion of the degeneracies and theoretical unknowns. In particular, we highlighted how better numerical simulations are needed to answer important and still open theoretical questions (Sect. 5.6).

While we only focused on galaxy-scale lenses, all of the approaches discussed above can potentially be extended to cluster-scale lenses. These type of studies would allows one to probe larger cosmological volumes and hence potentially require fewer observations to reach an equal level of constraints on dark matter. However, the lensing potential in galaxy clusters is significantly more complex than those of galaxies and it remains yet to be demonstrated that one can constrain their mass distribution with enough precision to avoid contamination by complex macro-models (see Sect. 5.1 for a discussion).

Currently, constraints on dark matter from lensing are based on relative small samples of systems (about ten for unresolved sources and about 50 for resolved ones). Ongoing and upcoming wide-sky surveys, with for example Euclid, the Vera Rubin Telescope, LOFAR and the SKA are expected to deliver orders of magnitudes more lensed galaxies and quasars. On the other hand, high-resolution follow-up with, for example, ALMA, the Global VLBI Network and the ELT will likely provide the data quality necessary to probe the dark matter distribution on small scales with resolved sources as well as obtain better constraints on the macro-model for unresolved ones. We can expect, therefore, that in the next five to ten years, the field of strong gravitational lensing will provide robust and statistically meaningful constraints on the nature of dark matter.

Funding Open Access funding enabled and organized by Projekt DEAL. S. V. thanks the Max Planck Society for support through a Max Planck Lise Meitner Group and funding from the European Research Council (ERC) under the European Union's Horizon 2020 research and innovation programme (LEDA: grant agreement No 758853). G. V. has received funding from the European Union's Horizon 2020 research and innovation programme under the Marie Sklodovska-Curie grant agreement No 897124. This research was made possible by the generosity of Eric and Wendy Schmidt by recommendation of the Schmidt Futures program. G. D. was supported by a Gliese Fellowship. C. D. F acknowledges support for this work from the National Science Foundation under Grant No. AST-1715611. D. G. was partially supported by a HQP grant from the McDonald Institute (reference number HQP 2019-4-2). Y. H. and L. P. are supported by a generous donation by Eric and Wendy Schmidt with the recommendation of the Schmidt Futures Foundation, as well as the National Sciences and Engineering Council of Canada, the Fonds de recherche du Québec, and the Canada Research Chairs Program. J. P. M. acknowledges support from the Netherlands Organization for Scientific Research (NWO, project number 629.001.023) and the Chinese Academy of Sciences (CAS, project number 114A11KYSB20170054). This work is based on the research supported in part by the National Research Foundation of South Africa (Grant Number: 128943).

Declarations

Competing Interests The authors declare no competing interests.

References

Abbott TMC et al [DES Collaboration] (eds) (2022) Dark Energy Survey Year 3 results: cosmological constraints from galaxy clustering and weak lensing. Phys Rev D 105(2):023520. https://doi.org/10.1103/PhysRevD.105.023520

Adam A, Coogan A, Malkin N, Legin R, Perreault-Levasseur L, Hezaveh Y, Bengio Y (2022) Posterior samples of source galaxies in strong gravitational lenses with score-based priors. ArXiv e-prints, arXiv:2211.03812 [astro-ph.IM]. https://doi.org/10.48550/arXiv.2211.03812

Adhikari S, Banerjee A, Boddy KK, Cyr-Racine F-Y, Desmond H, Dvorkin C, Jain B, Kahlhoefer F, Kaplinghat M, Nierenberg A, Peter AHG, Robertson A, Sakstein J, Zavala J (2022) Astrophysical Tests of Dark Matter Self-Interactions. ArXiv e-prints, arXiv:2207.10638 [astro-ph.CO]. https://doi.org/10.48550/arXiv.2207.10638

Alam S, Ata M, Bailey S, Beutler F, Bizyaev D, Blazek JA, Bolton AS, Brownstein JR, Burden A, Chuang C-H et al (2017) The clustering of galaxies in the completed SDSS-III Baryon Oscillation Spectroscopic Survey: cosmological analysis of the DR12 galaxy sample. Mon Not R Astron Soc 470(3):2617–2652

Alexander S, Gleyzer S, McDonough E, Toomey MW, Usai E (2020b) Deep learning the morphology of dark matter substructure. Astrophys J 893(1):15. https://doi.org/10.3847/1538-4357/ab7925

Alexander S, Gleyzer S, Parul H, Reddy P, Toomey MW, Usai E, Von Klar R (2020a) Decoding Dark Matter Substructure without Supervision. ArXiv e-prints, arXiv:2008.12731 [astro-ph.CO]. https://doi.org/10.48550/arXiv.2008.12731

Alexander S, Gleyzer S, Reddy P, Tidball M, Toomey MW (2021) Domain Adaptation for Simulation-Based Dark Matter Searches Using Strong Gravitational Lensing. ArXiv e-prints, arXiv:2112.12121 [astro-ph.CO]. https://doi.org/10.48550/arXiv.2112.12121

Amorisco NC, Nightingale J, He Q, Amvrosiadis A, Cao X, Cole S, Etherington A, Frenk CS, Li R, Massey R, Robertson A (2022) Halo concentration strengthens dark matter constraints in galaxy-galaxy strong lensing analyses. Mon Not R Astron Soc 510(2):2464–2479. https://doi.org/10.1093/mnras/stab3527

Amruth A, Broadhurst T, Lim J, Oguri M, Smoot GF, Diego JM, Leung E, Emami R, Li J, Chiueh T, Schive H-Y, Yeung MCH, Li Kei S (2023) Anomalies in Gravitational-Lensed Images revealing Einstein rings modulated by wavelike dark matter. Nat Astron 7:736. https://doi.org/10.1038/s41550-023-01943-9. arXiv:2304.09895 [astro-ph.CO]

Andrade KE, Fuson J, Gad-Nasr S, Kong D, Minor Q, Roberts MG, Kaplinghat M (2022) A stringent upper limit on dark matter self-interaction cross-section from cluster strong lensing. Mon Not R Astron Soc 510(1):54–81. https://doi.org/10.1093/mnras/stab3241

Angulo RE, Lacey CG, Baugh CM, Frenk CS (2009) The fate of substructures in cold dark matter haloes. Mon Not R Astron Soc 399(2):983–995. https://doi.org/10.1111/j.1365-2966.2009.15333.x

Arcadi G, Dutra M, Ghosh P, Lindner M, Mambrini Y, Pierre M, Profumo S, Queiroz FS (2018) The waning of the WIMP? A review of models, searches, and constraints. Eur Phys J C 78(3):203. https://doi.org/10.1140/epjc/s10052-018-5662-y

Auger MW, Treu T, Bolton AS, Gavazzi R, Koopmans LVE, Marshall PJ, Bundy K, Moustakas LA (2009) The Sloan Lens ACS Survey. IX. Colors, lensing, and stellar masses of early-type galaxies. Astrophys J 705(2):1099–1115. https://doi.org/10.1088/0004-637X/705/2/1099

Balberg S, Shapiro SL, Inagaki S (2002) Self-interacting dark matter halos and the gravothermal catastrophe. Astrophys J 568(2):475–487. https://doi.org/10.1086/339038

Banik N, Bovy J, Bertone G, Erkal D, de Boer TJL (2021) Novel constraints on the particle nature of dark matter from stellar streams. J Cosmol Astropart Phys 2021(10):043. https://doi.org/10.1088/1475-7516/2021/10/043

Bardeen JM, Bond JR, Kaiser N, Szalay AS (1986) The statistics of peaks of Gaussian random fields. Astrophys J 304:15–61. https://doi.org/10.1086/164143

Barnabè M, Nipoti C, Koopmans LVE, Vegetti S, Ciotti L (2009) Crash-testing the CAULDRON code for joint lensing and dynamics analysis of early-type galaxies. Mon Not R Astron Soc 393(4):1114–1126. https://doi.org/10.1111/j.1365-2966.2008.14208.x

Barnabè M, Czoske O, Koopmans LVE, Treu T, Bolton AS (2011) Two-dimensional kinematics of SLACS lenses - III. Mass structure and dynamics of early-type lens galaxies beyond z $\sim$ 0.1. Mon Not R Astron Soc 415(3):2215–2232. https://doi.org/10.1111/j.1365-2966.2011.18842.x

Basu A, Goswami J, Schwarz DJ, Urakawa Y (2021) Searching for axionlike particles under strong gravitational lenses. Phys Rev Lett 126(19):191102. https://doi.org/10.1103/PhysRevLett.126.191102

Bayer D, Chatterjee S, Koopmans LVE, Vegetti S, McKean JP, Treu T, Fassnacht CD, Glazebrook K (2023b) Probing sub-galactic mass structure with the power spectrum of surface-brightness anomalies in high-resolution observations of galaxy-galaxy strong gravitational lenses. II. Observational constraints on the subgalactic matter power spectrum. Mon Not R Astron Soc 523(1):1310–1325. https://doi.org/10.1093/mnras/stad1402

Bayer D, Koopmans LVE, McKean JP, Vegetti S, Treu T, Fassnacht CD, Glazebrook K (2023a) Probing sub-galactic mass structure with the power spectrum of surface-brightness anomalies in high-resolution observations of galaxy-galaxy strong gravitational lenses - I. Power-spectrum measurement and feasibility study. Mon Not R Astron Soc 523(1):1326–1345. https://doi.org/10.1093/mnras/stad1403

Belokurov V, Evans NW, Hewett PC, Moiseev A, McMahon RG, Sanchez SF, King LJ (2009) Two new large-separation gravitational lenses from SDSS. Mon Not R Astron Soc 392(1):104–112. https://doi.org/10.1111/j.1365-2966.2008.14075.x

Bennett CL, Lawrence CR, Burke BF, Hewitt JN, Mahoney J (1986) The MIT–Green Bank (MG) 5 GHz survey. Astrophys J Suppl Ser 61:1. https://doi.org/10.1086/191108

Berezinsky VS, Dokuchaev VI, Eroshenko YN (2014) Small-scale clumps of dark matter. Phys Usp 57(1):1–36. https://doi.org/10.3367/UFNe.0184.201401a.0003

Bertone G, Tait TMP (2018) A new era in the search for dark matter. Nature 562(7725):51–56. https://doi.org/10.1038/s41586-018-0542-z

Biggs AD (2023) A VLA monitoring study of JVAS B1422+231: investigation of time delays and detection of extrinsic variability. Mon Not R Astron Soc 522(1):426–437. https://doi.org/10.1093/mnras/stad870

Biggs AD, Browne IWA, Jackson NJ, York T, Norbury MA, McKean JP, Phillips PM (2004) Radio, optical and infrared observations of CLASS B0128+437. Mon Not R Astron Soc 350(3):949–961. https://doi.org/10.1111/j.1365-2966.2004.07701.x

Birrer S, Amara A, Refregier A (2015) Gravitational lens modeling with basis sets. Astrophys J 813(2):102. https://doi.org/10.1088/0004-637X/813/2/102

Birrer S, Amara A, Refregier A (2017) Lensing substructure quantification in RXJ1131-1231: a 2 keV lower bound on dark matter thermal relic mass. J Cosmol Astropart Phys 2017(5):037. https://doi.org/10.1088/1475-7516/2017/05/037

Bolton AS, Burles S, Koopmans LVE, Treu T, Gavazzi R, Moustakas LA, Wayth R, Schlegel DJ (2008) The Sloan Lens ACS Survey. V. The full ACS strong-lens sample. Astrophys J 682(2):964–984. https://doi.org/10.1086/589327

Bond JR, Cole S, Efstathiou G, Kaiser N (1991) Excursion set mass functions for hierarchical Gaussian fluctuations. Astrophys J 379:440–460. https://doi.org/10.1086/170520

Borsato E, Marchetti L, Negrello M, Corsini EM, Wake D, Amvrosiadis A, Baker AJ, Bakx TJLC, Beelen A, Berta S, Beyer A, Clements DL, Cooray A, Cox P, Dannerbauer H, de Zotti G, Dye S, Eales SA, Enia A, Farrah D, Gonzalez-Nuevo J, Hughes DH, Ismail D, Jin S, Lapi A, Lehnert MD, Neri R, Pérez-Fournon I, Riechers DA, Rodighiero G, Scott D, Serjeant S, Stanley F, Urquhart S, van der Werf P, Vaccari M, Wang L, Yang C, Young A (2024) Characterization of Herschel-selected strong lens candidates through HST and sub-mm/mm observations. Mon Not R Astron Soc 528(4):6222–6279. https://doi.org/10.1093/mnras/stad3381

Bose S, Hellwing WA, Frenk CS, Jenkins A, Lovell MR, Helly JC, Li B (2016) The Copernicus complexio: statistical properties of warm dark matter haloes. Mon Not R Astron Soc 455(1):318–333. https://doi.org/10.1093/mnras/stv2294

Boyarsky A, Ruchayskiy O, Shaposhnikov M (2009) The role of sterile neutrinos in cosmology and astrophysics. Annu Rev Nucl Part Sci 59(1):191–214. https://doi.org/10.1146/annurev.nucl.010909.083654

Boyarsky A, Drewes M, Lasserre T, Mertens S, Ruchayskiy O (2019) Sterile neutrino dark matter. Prog Part Nucl Phys 104:1–45. https://doi.org/10.1016/j.ppnp.2018.07.004

Bradač M, Schneider P, Steinmetz M, Lombardi M, King LJ, Porcas R (2002) B1422+231: the influence of mass substructure on strong lensing. Astron Astrophys 388:373–382. https://doi.org/10.1051/0004-6361:20020559

Bradač M, Schneider P, Lombardi M, Steinmetz M, Koopmans LVE, Navarro JF (2004) The signature of substructure on gravitational lensing in the ΛCDM cosmological model. Astron Astrophys 423:797–809. https://doi.org/10.1051/0004-6361:20040168

Brehmer J, Mishra-Sharma S, Hermans J, Louppe G, Cranmer K (2019) Mining for dark matter substructure: inferring subhalo population properties from strong lenses with machine learning. Astrophys J 886(1):49. https://doi.org/10.3847/1538-4357/ab4c41

Brewer BJ, Foreman-Mackey D, Hogg DW (2013) Probabilistic catalogs for crowded stellar fields. Astron J 146(1):7. https://doi.org/10.1088/0004-6256/146/1/7

Brewer BJ, Huijser D, Lewis GF (2016) Trans-dimensional Bayesian inference for gravitational lens substructures. Mon Not R Astron Soc 455(2):1819–1829. https://doi.org/10.1093/mnras/stv2370

Brooks AM, Kuhlen M, Zolotov A, Hooper D (2013) A baryonic solution to the missing satellites problem. Astrophys J 765(1):22. https://doi.org/10.1088/0004-637X/765/1/22

Browne IWA, Wilkinson PN, Patnaik AR, Wrobel JM (1998) Interferometer phase calibration sources - II. The region $0° \leq \delta_{B1950} \leq +20°$. Mon Not R Astron Soc 293(3):257–287. https://doi.org/10.1046/j.1365-8711.1998.01072.x

Browne IWA et al (2003) The Cosmic Lens All-Sky Survey - II. Gravitational lens candidate selection and follow-up. Mon Not R Astron Soc 341:13–32. https://doi.org/10.1046/j.1365-8711.2003.06257.x

Bryan GL, Norman ML (1998) Statistical properties of X-ray clusters: analytic and numerical comparisons. Astrophys J 495:80. https://doi.org/10.1086/305262

Bussmann RS, Gurwell MA, Fu H, Smith DJB, Dye S, Auld R, Baes M, Baker AJ, Bonfield D, Cava A, Clements DL, Cooray A, Coppin K, Dannerbauer H, Dariush A, De Zotti G, Dunne L, Eales S, Fritz J, Hopwood R, Ibar E, Ivison RJ, Jarvis MJ, Kim S, Leeuw LL, Maddox S, Michałowski MJ, Negrello M, Pascale E, Pohlen M, Riechers DA, Rigby E, Scott D, Temi P, Van der Werf PP, Wardlow J, Wilner D, Verma A (2012) A detailed gravitational lens model based on submillimeter array and Keck adaptive optics imaging of a Herschel-ATLAS submillimeter galaxy at z = 4.243. Astrophys J 756(2):134. https://doi.org/10.1088/0004-637X/756/2/134

Bussmann RS, Pérez-Fournon I, Amber S, Calanog J, Gurwell MA, Dannerbauer H, De Bernardis F, Fu H, Harris AI, Krips M, Lapi A, Maiolino R, Omont A, Riechers D, Wardlow J, Baker AJ, Birkinshaw M, Bock J, Bourne N, Clements DL, Cooray A, De Zotti G, Dunne L, Dye S, Eales S, Farrah D, Gavazzi R, González Nuevo J, Hopwood R, Ibar E, Ivison RJ, Laporte N, Maddox S, Martínez-Navajas P, Michalowski M, Negrello M, Oliver SJ, Roseboom IG, Scott D, Serjeant S, Smith AJ, Smith M, Streblyanska A, Valiante E, van der Werf P, Verma A, Vieira JD, Wang L, Wilner D (2013) Gravitational lens models based on submillimeter array imaging of Herschel-selected strongly lensed sub-millimeter galaxies at $z > 1.5$. Astrophys J 779(1):25. https://doi.org/10.1088/0004-637X/779/1/25

Cañameras R, Schuldt S, Shu Y, Suyu SH, Taubenberger S, Meinhardt T, Leal-Taixé L, Chao DC-Y, Inoue KT, Jaelani AT, More A (2021) HOLISMOKES. VI. New galaxy-scale strong lens candidates from the HSC-SSP imaging survey. Astron Astrophys 653:6. https://doi.org/10.1051/0004-6361/202141758

Casadio C, Blinov D, Readhead ACS, Browne IWA, Wilkinson PN, Hovatta T, Mandarakas N, Pavlidou V, Tassis K, Vedantham HK, Zensus JA, Diamantopoulos V, Dolapsaki KE, Gkimisi K, Kalaitzidakis G, Mastorakis M, Nikolaou K, Ntormousi E, Pelgrims V, Psarras K (2021) SMILE: search for MIlli-LEnses. Mon Not R Astron Soc 507(1):6–10. https://doi.org/10.1093/mnrasl/slab082

Chan JHH, Schive H-Y, Wong S-K, Chiueh T, Broadhurst T (2020) Multiple images and flux ratio anomaly of fuzzy gravitational lenses. Phys Rev Lett 125(11):111102. https://doi.org/10.1103/PhysRevLett.125.111102

Chan HYJ, Ferreira EGM, May S, Hayashi K, Chiba M (2022) The diversity of core-halo structure in the fuzzy dark matter model. Mon Not R Astron Soc 511(1):943–952. https://doi.org/10.1093/mnras/stac063

Chatterjee S, Koopmans LVE (2018) The inner mass power spectrum of galaxies using strong gravitational lensing: beyond linear approximation. Mon Not R Astron Soc 474(2):1762–1772. https://doi.org/10.1093/mnras/stx2674

Chen J (2009) Parity dependence in strong lens systems as a probe of dark matter substructure. Astron Astrophys 498(1):49–60. https://doi.org/10.1051/0004-6361/200811134

Chen J, Rozo E, Dalal N, Taylor JE (2007) Astrometric perturbations in substructure lensing. Astrophys J 659(1):52–68. https://doi.org/10.1086/512002

Chianese M, Coogan A, Hofma P, Otten S, Weniger C (2020) Differentiable strong lensing: uniting gravity and neural nets through differentiable probabilistic programming. Mon Not R Astron Soc 496(1):381–393. https://doi.org/10.1093/mnras/staa1477

Chiba M, Minezaki T, Kashikawa N, Kataza H, Inoue KT (2005) Subaru mid-infrared imaging of the quadruple lenses PG 1115+080 and B1422+231: limits on substructure lensing. Astrophys J 627(1):53–61. https://doi.org/10.1086/430403

Chua KTE, Pillepich A, Rodriguez-Gomez V, Vogelsberger M, Bird S, Hernquist L (2017) Subhalo demographics in the illustris simulation: effects of baryons and halo-to-halo variation. Mon Not R Astron Soc 472(4):4343–4360. https://doi.org/10.1093/mnras/stx2238

Clowe D, Bradač M, Gonzalez AH, Markevitch M, Randall SW, Jones C, Zaritsky D (2006) A direct empirical proof of the existence of dark matter. Astrophys J Lett 648(2):109–113. https://doi.org/10.1086/508162

Coogan A, Karchev K, Weniger C (2020) Targeted Likelihood-Free Inference of Dark Matter Substructure in Strongly-Lensed Galaxies. ArXiv e-prints, arXiv:2010.07032 [astro-ph.CO]

Cornwell TJ, Evans KF (1985) A simple maximum entropy deconvolution algorithm. Astron Astrophys 143(1):77–83

Correa CA (2021) Constraining velocity-dependent self-interacting dark matter with the Milky Way's dwarf spheroidal galaxies. Mon Not R Astron Soc 503(1):920–937. https://doi.org/10.1093/mnras/stab506

Cranmer K, Brehmer J, Louppe G (2020) The frontier of simulation-based inference. Proc Natl Acad Sci 117(48):30055–30062. https://doi.org/10.1073/pnas.1912789117

Cyr-Racine F-Y, Moustakas LA, Keeton CR, Sigurdson K, Gilman DA (2016) Dark census: statistically detecting the satellite populations of distant galaxies. Phys Rev D 94(4):043505. https://doi.org/10.1103/PhysRevD.94.043505

Cyr-Racine F-Y, Keeton CR, Moustakas LA (2019) Beyond subhalos: probing the collective effect of the universe's small-scale structure with gravitational lensing. Phys Rev D 100(2):023013. https://doi.org/10.1103/PhysRevD.100.023013

Dalal N, Kochanek CS (2002) Direct detection of cold dark matter substructure. Astrophys J 572(1):25–33. https://doi.org/10.1086/340303

Daylan T, Portillo SKN, Finkbeiner DP (2017) Inference of unresolved point sources at high galactic latitudes using probabilistic catalogs. Astrophys J 839(1):4. https://doi.org/10.3847/1538-4357/aa679e

Daylan T, Cyr-Racine F-Y, Diaz Rivero A, Dvorkin C, Finkbeiner DP (2018) Probing the small-scale structure in strongly lensed systems via transdimensional inference. Astrophys J 854(2):141. https://doi.org/10.3847/1538-4357/aaaa1e

Delos MS (2019) Evolution of dark matter microhalos through stellar encounters. Phys Rev D 100(8):083529. https://doi.org/10.1103/PhysRevD.100.083529

Despali G, Vegetti S (2017) The impact of baryonic physics on the subhalo mass function and implications for gravitational lensing. Mon Not R Astron Soc 469:1997–2010. https://doi.org/10.1093/mnras/stx966

Despali G, Giocoli C, Angulo RE, Tormen G, Sheth RK, Baso G, Moscardini L (2016) The universality of the virial halo mass function and models for non-universality of other halo definitions. Mon Not R Astron Soc 456:2486–2504. https://doi.org/10.1093/mnras/stv2842

Despali G, Vegetti S, White SDM, Giocoli C, van den Bosch FC (2018) Modelling the line-of-sight contribution in substructure lensing. Mon Not R Astron Soc 475(4):5424–5442. https://doi.org/10.1093/mnras/sty159

Despali G, Sparre M, Vegetti S, Vogelsberger M, Zavala J, Marinacci F (2019) The interplay of self-interacting dark matter and baryons in shaping the halo evolution. Mon Not R Astron Soc 484:4563–4573. https://doi.org/10.1093/mnras/stz273

Despali G, Lovell M, Vegetti S, Crain RA, Oppenheimer BD (2020) The lensing properties of subhaloes in massive elliptical galaxies in sterile neutrino cosmologies. Mon Not R Astron Soc 491(1):1295–1310. https://doi.org/10.1093/mnras/stz3068

Despali G, Vegetti S, White SDM, Powell DM, Stacey HR, Fassnacht CD, Rizzo F, Enzi W (2022) Detecting low-mass haloes with strong gravitational lensing I: the effect of data quality and lensing configuration. Mon Not R Astron Soc 510(2):2480–2494. https://doi.org/10.1093/mnras/stab3537

Dhanasingham B, Cyr-Racine F-Y, Peter AHG, Benson A, Gilman D (2022) Interlopers speak out: studying the dark universe using small-scale lensing anisotropies. Mon Not R Astron Soc. https://doi.org/10.1093/mnras/stac2993

Diaz Rivero A, Dvorkin C (2020) Direct detection of dark matter substructure in strong lens images with convolutional neural networks. Phys Rev D 101(2):023515. https://doi.org/10.1103/PhysRevD.101.023515

Diaz Rivero A, Cyr-Racine F-Y, Dvorkin C (2018) Power spectrum of dark matter substructure in strong gravitational lenses. Phys Rev D 97(2):023001. https://doi.org/10.1103/PhysRevD.97.023001

Díaz Rivero A, Dvorkin C, Cyr-Racine F-Y, Zavala J, Vogelsberger M (2018) Gravitational lensing and the power spectrum of dark matter substructure: insights from the ETHOS N-body simulations. Phys Rev D 98(10):103517. https://doi.org/10.1103/PhysRevD.98.103517

Diggle PJ, Gratton RJ (2018) Monte Carlo methods of inference for implicit statistical models. J R Stat Soc, Ser B, Methodol 46(2):193–212. https://doi.org/10.1111/j.2517-6161.1984.tb01290.x

Dobler G, Keeton CR (2006) Finite source effects in strong lensing: implications for the substructure mass scale. Mon Not R Astron Soc 365(4):1243–1262. https://doi.org/10.1111/j.1365-2966.2005.09809.x

Doroshkevich AG, Khlopov MI, Sunyaev RA, Szalay AS, Zeldovich IB (1981) Cosmological impact of the neutrino rest mass. Ann NY Acad Sci 375:32–42. https://doi.org/10.1111/j.1749-6632.1981.tb33688.x

Dubois Y, Beckmann R, Bournaud F, Choi H, Devriendt J, Jackson R, Kaviraj S, Kimm T, Kraljic K, Laigle C, Martin G, Park M-J, Peirani S, Pichon C, Volonteri M, Yi SK (2021) Introducing the NEWHORIZON simulation: galaxy properties with resolved internal dynamics across cosmic time. Astron Astrophys 651:109. https://doi.org/10.1051/0004-6361/202039429

Dye S, Furlanetto C, Dunne L, Eales SA, Negrello M, Nayyeri H, van der Werf PP, Serjeant S, Farrah D, Michałowski MJ, Baes M, Marchetti L, Cooray A, Riechers DA, Amvrosiadis A (2018) Modelling high-resolution ALMA observations of strongly lensed highly star-forming galaxies detected by Herschel. Mon Not R Astron Soc 476(4):4383–4394. https://doi.org/10.1093/mnras/sty513

Elíasdóttir Á, Hjorth J, Toft S, Burud I, Paraficz D (2006) Extinction curves of lensing galaxies out to z = 1. Astrophys J Suppl Ser 166(2):443–469. https://doi.org/10.1086/507131

Ellithorpe JD, Kochanek CS, Hewitt JN (1996) Visibility LensClean and the reliability of deconvolved radio images. Astrophys J 464:556. https://doi.org/10.1086/177346

Enzi W, Vegetti S, Despali G, Hsueh J-W, Metcalf RB (2020) Systematic errors in strong gravitational lensing reconstructions, a numerical simulation perspective. Mon Not R Astron Soc 496(2):1718–1729. https://doi.org/10.1093/mnras/staa1224

Enzi W, Murgia R, Newton O, Vegetti S, Frenk C, Viel M, Cautun M, Fassnacht CD, Auger M, Despali G, McKean J, Koopmans LVE, Lovell M (2021) Joint constraints on thermal relic dark matter from strong gravitational lensing, the Ly α forest, and Milky Way satellites. Mon Not R Astron Soc 506(4):5848–5862. https://doi.org/10.1093/mnras/stab1960

Erkal D, Koposov SE, Belokurov V (2017) A sharper view of Pal 5's tails: discovery of stream perturbations with a novel non-parametric technique. Mon Not R Astron Soc 470(1):60–84. https://doi.org/10.1093/mnras/stx1208

Ettori S, Donnarumma A, Pointecouteau E, Reiprich TH, Giodini S, Lovisari L, Schmidt RW (2013) Mass profiles of galaxy clusters from X-ray analysis. Space Sci Rev 177(1–4):119–154. https://doi.org/10.1007/s11214-013-9976-7

Fassnacht CD, Blandford RD, Cohen JG, Matthews K, Pearson TJ, Readhead ACS, Womble DS, Myers ST, Browne IWA, Jackson NJ, Marlow DR, Wilkinson PN, Koopmans LVE, de Bruyn AG, Schilizzi RT, Bremer M, Miley G (1999) B2045+265: a new four-image gravitational lens from CLASS. Astron J 117(2):658–670. https://doi.org/10.1086/300724

Fassnacht CD, Xanthopoulos E, Koopmans LVE, Rusin D (2002) A determination of H_0 with the CLASS gravitational lens B1608+656. III. A significant improvement in the precision of the time delay measurements. Astrophys J 581(2):823–835. https://doi.org/10.1086/344368

Feng JL (2010) Dark matter candidates from particle physics and methods of detection. Annu Rev Astron Astrophys 48:495–545. https://doi.org/10.1146/annurev-astro-082708-101659

Feng W-X, Yu H-B, Zhong Y-M (2021) Seeding supermassive black holes with self-interacting dark matter: a unified scenario with baryons. Astrophys J Lett 914(2):26. https://doi.org/10.3847/2041-8213/ac04b0

Fox PJ (2018) TASI Lectures on WIMPs and Supersymmetry. PoS(TASI2028)005. https://doi.org/10.22323/1.333.0005

Galan A, Vernardos G, Peel A, Courbin F, Starck J-L (2022) Using wavelets to capture deviations from smoothness in galaxy-scale strong lenses. Astron Astrophys 668:155. https://doi.org/10.1051/0004-6361/202244464

Gao L, White SDM, Jenkins A, Stoehr F, Springel V (2004) The subhalo populations of ΛCDM dark haloes. Mon Not R Astron Soc 355(3):819–834. https://doi.org/10.1111/j.1365-2966.2004.08360.x

Gao L, Navarro JF, Frenk CS, Jenkins A, Springel V, White SDM (2012) The Phoenix project: the dark side of rich galaxy clusters. Mon Not R Astron Soc 425(3):2169–2186. https://doi.org/10.1111/j.1365-2966.2012.21564.x

Garrison-Kimmel S, Hopkins PF, Wetzel A, Bullock JS, Boylan-Kolchin M, Kereš D, Faucher-Giguère C-A, El-Badry K, Lamberts A, Quataert E, Sanderson R (2019) The local group on FIRE: dwarf galaxy populations across a suite of hydrodynamic simulations. Mon Not R Astron Soc 487(1):1380–1399. https://doi.org/10.1093/mnras/stz1317

Gilman D, Agnello A, Treu T, Keeton CR, Nierenberg AM (2017) Strong lensing signatures of luminous structure and substructure in early-type galaxies. Mon Not R Astron Soc 467(4):3970–3992. https://doi.org/10.1093/mnras/stx158

Gilman D, Birrer S, Treu T, Keeton CR, Nierenberg A (2018) Probing the nature of dark matter by forward modelling flux ratios in strong gravitational lenses. Mon Not R Astron Soc 481(1):819–834. https://doi.org/10.1093/mnras/sty2261

Gilman D, Birrer S, Treu T, Nierenberg A, Benson A (2019) Probing dark matter structure down to 10^7 solar masses: flux ratio statistics in gravitational lenses with line-of-sight haloes. Mon Not R Astron Soc 487(4):5721–5738. https://doi.org/10.1093/mnras/stz1593

Gilman D, Birrer S, Nierenberg A, Treu T, Du X, Benson A (2020b) Warm dark matter chills out: constraints on the halo mass function and the free-streaming length of dark matter with eight quadruple-image strong gravitational lenses. Mon Not R Astron Soc 491(4):6077–6101. https://doi.org/10.1093/mnras/stz3480

Gilman D, Birrer S, Treu T (2020) TDCOSMO. III. Dark matter substructure meets dark energy. The effects of (sub)halos on strong-lensing measurements of H_0. Astron Astrophys 642:194. https://doi.org/10.1051/0004-6361/202038829

Gilman D, Du X, Benson A, Birrer S, Nierenberg A, Treu T (2020a) Constraints on the mass-concentration relation of cold dark matter halos with 11 strong gravitational lenses. Mon Not R Astron Soc 492(1):12–16. https://doi.org/10.1093/mnrasl/slz173

Gilman D, Bovy J, Treu T, Nierenberg A, Birrer S, Benson A, Sameie O (2021) Strong lensing signatures of self-interacting dark matter in low-mass haloes. Mon Not R Astron Soc 507(2):2432–2447. https://doi.org/10.1093/mnras/stab2335

Gilman D, Benson A, Bovy J, Birrer S, Treu T, Nierenberg A (2022) The primordial matter power spectrum on sub-galactic scales. Mon Not R Astron Soc 512(3):3163–3188. https://doi.org/10.1093/mnras/stac670

Gilman D, Zhong Y-M, Bovy J (2022) Constraining resonant dark matter self-interactions with strong gravitational lenses. ArXiv e-prints, 2207–13111. https://doi.org/10.48550/arXiv.2207.13111

Giocoli C, Pieri L, Tormen G (2008) Analytical approach to subhalo population in dark matter haloes. Mon Not R Astron Soc 387:689–697. https://doi.org/10.1111/j.1365-2966.2008.13283.x

Green PJ (1995) Reversible jump Markov chain Monte Carlo computation and Bayesian model determination. Biometrika 82(4):711–732. https://doi.org/10.1093/biomet/82.4.711

Green PJ (2003) Trans-dimensional Markov chain Monte Carlo. In: Green PJ, Hjort NL, Richardson S (eds) Highly structured stochastic systems. Oxford University Press, Oxford, pp 179–198. https://doi.org/10.1093/oso/9780198510550.003.0017

Green AM, Kavanagh BJ (2021) Primordial black holes as a dark matter candidate. J Phys G, Nucl Phys 48(4):043001. https://doi.org/10.1088/1361-6471/abc534

Green SB, van den Bosch FC (2019) The tidal evolution of dark matter substructure - I. subhalo density profiles. Mon Not R Astron Soc 490(2):2091–2101. https://doi.org/10.1093/mnras/stz2767

Green SB, van den Bosch FC, Jiang F (2021) The tidal evolution of dark matter substructure - II. The impact of artificial disruption on subhalo mass functions and radial profiles. Mon Not R Astron Soc 503(3):4075–4091. https://doi.org/10.1093/mnras/stab696

Griffith M, Langston G, Heflin M, Conner S, Lehar J, Burke B (1990) The third MIT–Green Bank 5 GHz survey. Astrophys J Suppl Ser 74:129. https://doi.org/10.1086/191495

Griffith M, Langston G, Heflin M, Conner S, Burke B (1991) The fourth MIT–Green Bank 5 GHz survey. Astrophys J Suppl Ser 75:801. https://doi.org/10.1086/191549

He Q, Nightingale J, Robertson A, Amvrosiadis A, Cole S, Frenk CS, Massey R, Li R, Amorisco NC, Metcalf RB, Cao X, Etherington A (2023) Testing strong lensing subhalo detection with a cosmological simulation. Mon Not R Astron Soc 518(1):220–239. https://doi.org/10.1093/mnras/stac2779

Heinze FM, Despali G, Klessen RS (2023) Not all subhaloes are created equal: modelling the diversity of subhalo density profiles in TNG50. Mon Not R Astron Soc 527(4):11996–12015. https://doi.org/10.1093/mnras/stad3894

Heymans C, Tröster T, Asgari M, Blake C, Hildebrandt H, Joachimi B, Kuijken K, Lin C-A, Sánchez AG, van den Busch JL, Wright AH, Amon A, Bilicki M, de Jong J, Crocce M, Dvornik A, Erben T, Fortuna MC, Getman F, Giblin B, Glazebrook K, Hoekstra H, Joudaki S, Kannawadi A, Köhlinger F, Lidman C, Miller L, Napolitano NR, Parkinson D, Schneider P, Shan H, Valentijn EA, Verdoes Kleijn G, Wolf C (2021) KiDS-1000 cosmology: multi-probe weak gravitational lensing and spectroscopic galaxy clustering constraints. Astron Astrophys 646:140. https://doi.org/10.1051/0004-6361/202039063

Hezaveh Y, Dalal N, Holder G, Kuhlen M, Marrone D, Murray N, Vieira J (2013) Dark matter substructure detection using spatially resolved spectroscopy of lensed dusty galaxies. Astrophys J 767(1):9. https://doi.org/10.1088/0004-637X/767/1/9

Hezaveh YD, Marrone DP, Fassnacht CD, Spilker JS, Vieira JD, Aguirre JE, Aird KA, Aravena M, Ashby MLN, Bayliss M, Benson BA, Bleem LE, Bothwell M, Brodwin M, Carlstrom JE, Chang CL, Chapman SC, Crawford TM, Crites AT, De Breuck C, de Haan T, Dobbs MA, Fomalont EB, George EM, Gladders MD, Gonzalez AH, Greve TR, Halverson NW, High FW, Holder GP, Holzapfel WL, Hoover S, Hrubes JD, Husband K, Hunter TR, Keisler R, Lee AT, Leitch EM, Lueker M, Luong-Van D, Malkan M, McIntyre V, McMahon JJ, Mehl J, Menten KM, Meyer SS, Mocanu LM, Murphy EJ, Natoli T, Padin S, Plagge T, Reichardt CL, Rest A, Ruel J, Ruhl JE, Sharon K, Schaffer KK, Shaw L, Shirokoff E, Stalder B, Staniszewski Z, Stark AA, Story K, Vanderlinde K, Weiß A, Welikala N, Williamson R (2013) ALMA observations of SPT-discovered, strongly lensed, dusty, star-forming galaxies. Astrophys J 767(2):132. https://doi.org/10.1088/0004-637X/767/2/132

Hezaveh Y, Dalal N, Holder G, Kisner T, Kuhlen M, Perreault Levasseur L (2016) Measuring the power spectrum of dark matter substructure using strong gravitational lensing. J Cosmol Astropart Phys 2016(11):048. https://doi.org/10.1088/1475-7516/2016/11/048

Hezaveh YD, Dalal N, Marrone DP, Mao Y-Y, Morningstar W, Wen D, Blandford RD, Carlstrom JE, Fassnacht CD, Holder GP, Kemball A, Marshall PJ, Murray N, Perreault Levasseur L, Vieira JD, Wechsler RH (2016) Detection of lensing substructure using ALMA observations of the dusty galaxy SDP.81. Astrophys J 823:37. https://doi.org/10.3847/0004-637X/823/1/37

Hezaveh YD, Perreault Levasseur L, Marshall PJ (2017) Fast automated analysis of strong gravitational lenses with convolutional neural networks. Nature 548(7669):555–557. https://doi.org/10.1038/nature23463

Högbom JA (1974) Aperture synthesis with a non-regular distribution of interferometer baselines. Astron Astrophys Suppl Ser 15:417

Hogg DW, Lang D (2010) Telescopes don't make catalogues! In: Turon C, Meynadier F, Arenou F (eds). GAIA: at the frontiers of astrometry. EAS Publications Series, vol 45, pp 351–358. https://doi.org/10.1051/eas/1045059

Holzschuh BJ, O'Riordan CM, Vegetti S, Rodriguez-Gomez V, Thuerey N (2022) Realistic galaxy images and improved robustness in machine learning tasks from generative modelling. Mon Not R Astron Soc 515(1):652–677. https://doi.org/10.1093/mnras/stac1188

Hsueh J-W, Fassnacht CD, Vegetti S, McKean JP, Spingola C, Auger MW, Koopmans LVE, Lagattuta DJ (2016) SHARP - II. Mass structure in strong lenses is not necessarily dark matter substructure: a flux ratio anomaly from an edge-on disc in B1555+375. Mon Not R Astron Soc 463(1):51–55. https://doi.org/10.1093/mnrasl/slw146

Hsueh J-W, Oldham L, Spingola C, Vegetti S, Fassnacht CD, Auger MW, Koopmans LVE, McKean JP, Lagattuta DJ (2017) SHARP - IV. An apparent flux-ratio anomaly resolved by the edge-on disc in B0712+472. Mon Not R Astron Soc 469(3):3713–3721. https://doi.org/10.1093/mnras/stx1082

Hsueh J-W, Despali G, Vegetti S, Xu D, Fassnacht CD, Metcalf RB (2018) Flux-ratio anomalies from discs and other baryonic structures in the illustris simulation. Mon Not R Astron Soc 475(2):2438–2451. https://doi.org/10.1093/mnras/stx3320

Hsueh J-W, Enzi W, Vegetti S, Auger MW, Fassnacht CD, Despali G, Koopmans LVE, McKean JP (2020) SHARP - VII. New constraints on the dark matter free-streaming properties and substructure abundance from gravitationally lensed quasars. Mon Not R Astron Soc 492(2):3047–3059. https://doi.org/10.1093/mnras/stz3177

Huang X, Storfer C, Gu A, Ravi V, Pilon A, Sheu W, Venguswamy R, Banka S, Dey A, Landriau M, Lang D, Meisner A, Moustakas J, Myers AD, Sajith R, Schlafly EF, Schlegel DJ (2021) Discovering new strong gravitational lenses in the DESI Legacy Imaging Surveys. Astrophys J 909(1):27. https://doi.org/10.3847/1538-4357/abd62b

Hui L (2021) Wave dark matter. Annu Rev Astron Astrophys 59:247–289. https://doi.org/10.1146/annurev-astro-120920-010024

Inoue KT, Minezaki T, Matsushita S, Chiba M (2016) ALMA imprint of intergalactic dark structures in the gravitational lens SDP.81. Mon Not R Astron Soc 457(3):2936–2950. https://doi.org/10.1093/mnras/stw168

Iršič V, Viel M, Haehnelt MG, Bolton JS, Becker GD (2017) First constraints on fuzzy dark matter from Lyman-α forest data and hydrodynamical simulations. Phys Rev Lett 119(3):031302. https://doi.org/10.1103/PhysRevLett.119.031302

Kaplinghat M, Keeley RE, Linden T, Yu H-B (2014) Tying dark matter to baryons with self-interactions. Phys Rev Lett 113(2):021302. https://doi.org/10.1103/PhysRevLett.113.021302

Kaplinghat M, Valli M, Yu H-B (2019) Too big to fail in light of Gaia. Mon Not R Astron Soc 490(1):231–242. https://doi.org/10.1093/mnras/stz2511

Kaplinghat M, Ren T, Yu H-B (2020) Dark matter cores and cusps in spiral galaxies and their explanations. J Cosmol Astropart Phys 2020(6):027. https://doi.org/10.1088/1475-7516/2020/06/027

Karchev K, Coogan A, Weniger C (2022) Strong-lensing source reconstruction with variationally optimized Gaussian processes. Mon Not R Astron Soc 512(1):661–685. https://doi.org/10.1093/mnras/stac311

Kawai H, Oguri M, Amruth A, Broadhurst T, Lim J (2022) An analytic model for the subgalactic matter power spectrum in fuzzy dark matter halos. Astrophys J 925(1):61. https://doi.org/10.3847/1538-4357/ac39a2

Keeton CR, Moustakas LA (2009) A new channel for detecting dark matter substructure in galaxies: gravitational lens time delays. Astrophys J 699(2):1720–1731. https://doi.org/10.1088/0004-637X/699/2/1720

Knebe A, Knollmann SR, Muldrew SI, Pearce FR, Aragon-Calvo MA, Ascasibar Y, Behroozi PS, Ceverino D et al (2011) Haloes gone MAD: the halo-finder comparison project. Mon Not R Astron Soc 415:2293–2318. https://doi.org/10.1111/j.1365-2966.2011.18858.x

Knebe A, Pearce FR, Lux H, Ascasibar Y, Behroozi P, Casado J, Moran CC, Diemand J et al (2013) Structure finding in cosmological simulations: the state of affairs. Mon Not R Astron Soc 435:1618–1658. https://doi.org/10.1093/mnras/stt1403

Kochanek CS, Narayan R (1992) LensClean: an algorithm for inverting extended, gravitationally lensed images with application to the radio ring lens PKS 1830-211. Astrophys J 401:461. https://doi.org/10.1086/172078

Koopmans LVE (2005) Gravitational imaging of cold dark matter substructures. Mon Not R Astron Soc 363(4):1136–1144. https://doi.org/10.1111/j.1365-2966.2005.09523.x

Koopmans LVE, de Bruyn AG (2000) Microlensing of multiply-imaged compact radio sources. Evidence for compact halo objects in the disk galaxy of B1600+434. Astron Astrophys 358:793–811. https://doi.org/10.48550/arXiv.astro-ph/0004112

Koopmans LVE, Biggs A, Blandford RD, Browne IWA, Jackson NJ, Mao S, Wilkinson PN, de Bruyn AG, Wambsganss J (2003) Extrinsic radio variability of JVAS/CLASS gravitational lenses. Astrophys J 595(2):712–718. https://doi.org/10.1086/377434

Koopmans LVE, Bolton A, Treu T, Czoske O, Auger MW, Barnabè M, Vegetti S, Gavazzi R, Moustakas LA, Burles S (2009) The structure and dynamics of massive early-type galaxies: on homology, isothermality, and isotropy inside one effective radius. Astrophys J Lett 703(1):51–54. https://doi.org/10.1088/0004-637X/703/1/L51

Kulkarni M, Ostriker JP (2022) What is the halo mass function in a fuzzy dark matter cosmology? Mon Not R Astron Soc 510(1):1425–1430. https://doi.org/10.1093/mnras/stab3520
Lagattuta DJ, Vegetti S, Fassnacht CD, Auger MW, Koopmans LVE, McKean JP (2012) SHARP - I. A high-resolution multiband view of the infrared Einstein ring of JVAS B1938+666. Mon Not R Astron Soc 424(4):2800–2810. https://doi.org/10.1111/j.1365-2966.2012.21406.x
Langston GI, Heflin MB, Conner SR, Lehar J, Carilli CL, Burke BF (1990) The second MIT–green bank 5 GHz survey. Astrophys J Suppl Ser 72:621. https://doi.org/10.1086/191427
Lanusse F, Ma Q, Li N, Collett TE, Li C-L, Ravanbakhsh S, Mandelbaum R, Póczos B (2018) CMU DeepLens: deep learning for automatic image-based galaxy-galaxy strong lens finding. Mon Not R Astron Soc 473(3):3895–3906. https://doi.org/10.1093/mnras/stx1665
Laroche A, Gilman D, Li X, Bovy J, Du X (2022) Quantum fluctuations masquerade as haloes: bounds on ultra-light dark matter from quadruply imaged quasars. Mon Not R Astron Soc 517(2):1867–1883. https://doi.org/10.1093/mnras/stac2677
Legin R, Stone C, Hezaveh Y, Perreault-Levasseur L (2022) Population-Level Inference of Strong Gravitational Lenses with Neural Network-Based Selection Correction. ArXiv e-prints, arXiv:2207.04123 [astro-ph.IM]. https://doi.org/10.48550/arXiv.2207.04123
Li R, Frenk CS, Cole S, Wang Q, Gao L (2017) Projection effects in the strong lensing study of subhaloes. Mon Not R Astron Soc 468(2):1426–1432. https://doi.org/10.1093/mnras/stx554
Liepe J, Kirk P, Filippi S, Toni T, Barnes CP, Stumpf MPH (2014) A framework for parameter estimation and model selection from experimental data in systems biology using approximate Bayesian computation. Nat Protoc 9:439–456. https://doi.org/10.1038/nprot.2014.025
Loudas N, Pavlidou V, Casadio C, Tassis K (2022) Discriminating power of milli-lensing observations for dark matter models. Astron Astrophys 668:166. https://doi.org/10.1051/0004-6361/202244978
Lovell MR (2020) The halo mass function in alternative dark matter models. Mon Not R Astron Soc 493(1):11–15. https://doi.org/10.1093/mnrasl/slaa005
Lovell MR (2020) Toward a general parameterization of the warm dark matter halo mass function. Astrophys J 897(2):147. https://doi.org/10.3847/1538-4357/ab982a
Lovell MR, Eke V, Frenk CS, Gao L, Jenkins A, Theuns T, Wang J, White SDM, Boyarsky A, Ruchayskiy O (2012) The haloes of bright satellite galaxies in a warm dark matter universe. Mon Not R Astron Soc 420:2318–2324. https://doi.org/10.1111/j.1365-2966.2011.20200.x
Lovell MR, Frenk CS, Eke VR, Jenkins A, Gao L, Theuns T (2014) The properties of warm dark matter haloes. Mon Not R Astron Soc 439(1):300–317. https://doi.org/10.1093/mnras/stt2431
Lovell MR, Zavala J, Vogelsberger M (2019) ETHOS - an effective theory of structure formation: formation of the first haloes and their stars. Mon Not R Astron Soc 485(4):5474–5489. https://doi.org/10.1093/mnras/stz766
Ludlow AD, Bose S, Angulo RE, Wang L, Hellwing WA, Navarro JF, Cole S, Frenk CS (2016) The mass-concentration-redshift relation of cold and warm dark matter haloes. Mon Not R Astron Soc 460:1214–1232. https://doi.org/10.1093/mnras/stw1046
Mandelbaum R, Seljak U, Kauffmann G, Hirata CM, Brinkmann J (2006) Galaxy halo masses and satellite fractions from galaxy-galaxy lensing in the Sloan Digital Sky Survey: stellar mass, luminosity, morphology and environment dependencies. Mon Not R Astron Soc 368(2):715–731. https://doi.org/10.1111/j.1365-2966.2006.10156.x
Mao S, Schneider P (1998) Evidence for substructure in lens galaxies? Mon Not R Astron Soc 295(3):587–594. https://doi.org/10.1046/j.1365-8711.1998.01319.x
Mao S, Jing Y, Ostriker JP, Weller J (2004) Anomalous flux ratios in gravitational lenses: for or against cold dark matter? Astrophys J Lett 604(1):5–8. https://doi.org/10.1086/383413
Marlow DR, Myers ST, Rusin D, Jackson N, Browne IWA, Wilkinson PN, Muxlow T, Fassnacht CD, Lubin L, Kundić T, Blandford RD, Pearson TJ, Readhead ACS, Koopmans L, de Bruyn AG (1999) CLASS B1555+375: a new four-image gravitational lens system. Astron J 118(2):654–658. https://doi.org/10.1086/300987
Marsh DJE, Niemeyer JC (2019) Strong constraints on fuzzy dark matter from ultrafaint dwarf galaxy eridanus II. Phys Rev Lett 123(5):051103. https://doi.org/10.1103/PhysRevLett.123.051103
Marsh DJE, Silk J (2014) A model for halo formation with axion mixed dark matter. Mon Not R Astron Soc 437(3):2652–2663. https://doi.org/10.1093/mnras/stt2079
May S, Springel V (2021) Structure formation in large-volume cosmological simulations of fuzzy dark matter: impact of the non-linear dynamics. Mon Not R Astron Soc 506(2):2603–2618. https://doi.org/10.1093/mnras/stab1764
May S, Springel V (2023) The halo mass function and filaments in full cosmological simulations with fuzzy dark matter. Mon Not R Astron Soc 524(3):4256–4274. https://doi.org/10.1093/mnras/stad2031
McKean JP, Koopmans LVE, Flack CE, Fassnacht CD, Thompson D, Matthews K, Blandford RD, Readhead ACS, Soifer BT (2007) High-resolution imaging of the anomalous flux ratio gravitational lens system

CLASS B2045+265: dark or luminous satellites? Mon Not R Astron Soc 378(1):109–118. https://doi.org/10.1111/j.1365-2966.2007.11744.x
McKean J, Jackson N, Vegetti S, Rybak M, Serjeant S, Koopmans LVE, Metcalf RB, Fassnacht C, Marshall PJ, Pandey-Pommier M (2015) Strong gravitational lensing with the SKA. In: Advancing Astrophysics with the Square Kilometre Array (AASKA14), p 84
Metcalf RB, Moustakas LA, Bunker AJ, Parry IR (2004) Spectroscopic gravitational lensing and limits on the dark matter substructure in Q2237+0305. Astrophys J 607(1):43–59. https://doi.org/10.1086/383243
Minor Q, Gad-Nasr S, Kaplinghat M, Vegetti S (2021) An unexpected high concentration for the dark substructure in the gravitational lens SDSSJ0946+1006. Mon Not R Astron Soc 507(2):1662–1683. https://doi.org/10.1093/mnras/stab2247
Mittal R, Porcas R, Wucknitz O (2007) Free-free absorption in the gravitational lens JVAS B0218+357. Astron Astrophys 465(2):405–415. https://doi.org/10.1051/0004-6361:20066127
Mocz P, Fialkov A, Vogelsberger M, Becerra F, Amin MA, Bose S, Boylan-Kolchin M, Chavanis P-H, Hernquist L, Lancaster L, Marinacci F, Robles VH, Zavala J (2019) First star-forming structures in fuzzy cosmic filaments. Phys Rev Lett 123(14):141301. https://doi.org/10.1103/PhysRevLett.123.141301
Moliné Á, Sánchez-Conde MA, Palomares-Ruiz S, Prada F (2017) Characterization of subhalo structural properties and implications for dark matter annihilation signals. Mon Not R Astron Soc 466:4974–4990. https://doi.org/10.1093/mnras/stx026
Montel NA, Coogan A, Correa C, Karchev K, Weniger C (2022) Estimating the warm dark matter mass from strong lensing images with truncated marginal neural ratio estimation. Mon Not R Astron Soc. https://doi.org/10.1093/mnras/stac3215
Moustakas LA, Metcalf RB (2003) Detecting dark matter substructure spectroscopically in strong gravitational lenses. Mon Not R Astron Soc 339(3):607–615. https://doi.org/10.1046/j.1365-8711.2003.06055.x
Mukherjee S, Koopmans LVE, Metcalf RB, Tortora C, Schaller M, Schaye J, Vernardos G, Bellagamba F (2021) SEAGLE - II. Constraints on feedback models in galaxy formation from massive early-type strong-lens galaxies. Mon Not R Astron Soc 504(3):3455–3477. https://doi.org/10.1093/mnras/stab693
Müller-Sánchez F, Prieto MA, Hicks EKS, Vives-Arias H, Davies RI, Malkan M, Tacconi LJ, Genzel R (2011) Outflows from active galactic nuclei: kinematics of the narrow-line and coronal-line regions in seyfert galaxies. Astrophys J 739(2):69. https://doi.org/10.1088/0004-637X/739/2/69
Myers ST, Jackson NJ, Browne IWA, de Bruyn AG, Pearson TJ, Readhead ACS, Wilkinson PN, Biggs AD, Blandford RD, Fassnacht CD, Koopmans LVE, Marlow DR, McKean JP, Norbury MA, Phillips PM, Rusin D, Shepherd MC, Sykes CM (2003) The cosmic lens all-sky survey - I. Source selection and observations. Mon Not R Astron Soc 341:1–12. https://doi.org/10.1046/j.1365-8711.2003.06256.x
Nadler EO, Banerjee A, Adhikari S, Mao Y-Y, Wechsler RH (2020) Signatures of velocity-dependent dark matter self-interactions in Milky Way-mass halos. Astrophys J 896(2):112. https://doi.org/10.3847/1538-4357/ab94b0
Nadler EO, Birrer S, Gilman D, Wechsler RH, Du X, Benson A, Nierenberg AM, Treu T (2021) Dark matter constraints from a unified analysis of strong gravitational lenses and Milky Way satellite galaxies. Astrophys J 917(1):7. https://doi.org/10.3847/1538-4357/abf9a3
Nadler EO, Drlica-Wagner A, Bechtol K, Mau S, Wechsler RH, Gluscevic V, Boddy K, Pace AB, Li TS, McNanna M, Riley AH, García-Bellido J, Mao Y-Y, Green G, Burke DL, Peter A, Jain B, Abbott TMC, Aguena M, Allam S, Annis J, Avila S, Brooks D, Carrasco Kind M, Carretero J, Costanzi M, da Costa LN, De Vicente J, Desai S, Diehl HT, Doel P, Everett S, Evrard AE, Flaugher B, Frieman J, Gerdes DW, Gruen D, Gruendl RA, Gschwend J, Gutierrez G, Hinton SR, Honscheid K, Huterer D, James DJ, Krause E, Kuehn K, Kuropatkin N, Lahav O, Maia MAG, Marshall JL, Menanteau F, Miquel R, Palmese A, Paz-Chinchón F, Plazas AA, Romer AK, Sanchez E, Scarpine V, Serrano S, Sevilla-Noarbe I, Smith M, Soares-Santos M, Suchyta E, Swanson MEC, Tarle G, Tucker DL, Walker AR, Wester W (2021) Constraints on dark matter properties from observations of Milky Way satellite galaxies. Phys Rev Lett 126:091101. https://doi.org/10.1103/PhysRevLett.126.091101
Navarro JF, Frenk CS, White SDM (1996) The structure of cold dark matter halos. Astrophys J 462:563. https://doi.org/10.1086/177173
Nierenberg AM, Treu T, Wright SA, Fassnacht CD, Auger MW (2014) Detection of substructure with adaptive optics integral field spectroscopy of the gravitational lens B1422+231. Mon Not R Astron Soc 442(3):2434–2445. https://doi.org/10.1093/mnras/stu862
Nierenberg AM, Treu T, Brammer G, Peter AHG, Fassnacht CD, Keeton CR, Kochanek CS, Schmidt KB, Sluse D, Wright SA (2017) Probing dark matter substructure in the gravitational lens HE 0435-1223 with the WFC3 grism. Mon Not R Astron Soc 471(2):2224–2236. https://doi.org/10.1093/mnras/stx1400
Nierenberg AM, Gilman D, Treu T, Brammer G, Birrer S, Moustakas L, Agnello A, Anguita T, Fassnacht CD, Motta V, Peter AHG, Sluse D (2020) Double dark matter vision: twice the number of compact-source lenses with narrow-line lensing and the WFC3 grism. Mon Not R Astron Soc 492(4):5314–5335. https://doi.org/10.1093/mnras/stz358810.48550/arXiv.1908.06344

Nierenberg A, Bennert VN, Benson A, Birrer S, Djorgovski SG, Du X, Fassnacht C, Gilman D, Hoenig SF, Kusenko A, Malkan MA, Motta V, Moustakas LA, Sluse D, Stern DK, Treu TL (2021) A definitive test of the dark matter paradigm on small scales. JWST Proposal Cycle 1:#2046

Nightingale JW, Dye S (2015) Adaptive semi-linear inversion of strong gravitational lens imaging. Mon Not R Astron Soc 452(3):2940–2959. https://doi.org/10.1093/mnras/stv1455

Nightingale JW, He Q, Cao X, Amvrosiadis A, Etherington A, Frenk CS, Hayes RG, Robertson A, Cole S, Lange S, Li R, Massey R (2022) Scanning for Dark Matter Subhalos in Hubble Space Telescope Imaging of 54 Strong Lenses. ArXiv e-prints, arXiv:2209.10566 [astro-ph.CO]

Nishikawa H, Boddy KK, Kaplinghat M (2020) Accelerated core collapse in tidally stripped self-interacting dark matter halos. Phys Rev D 101(6):063009

Oguri M, Marshall PJ (2010) Gravitationally lensed quasars and supernovae in future wide-field optical imaging surveys. Mon Not R Astron Soc 405(4):2579–2593. https://doi.org/10.1111/j.1365-2966.2010.16639.x

Okabe N, Smith GP, Umetsu K, Takada M, Futamase T (2013) LoCuSS: the mass density profile of massive galaxy clusters at z = 0.2. Astrophys J Lett 769:35. https://doi.org/10.1088/2041-8205/769/2/L35

Onions J, Knebe A, Pearce FR, Muldrew SI, Lux H, Knollmann SR, Ascasibar Y, Behroozi P, Elahi P, Han J, Maciejewski M, Merchán ME, Neyrinck M, Ruiz AN, Sgró MA, Springel V, Tweed D (2012) Subhaloes going notts: the subhalo-finder comparison project. Mon Not R Astron Soc 423:1200–1214. https://doi.org/10.1111/j.1365-2966.2012.20947.x

O'Riordan CM, Vegetti S (2024) Angular complexity in strong lens substructure detection. Mon Not R Astron Soc 528(2):1757–1768. https://doi.org/10.1093/mnras/stae153

O'Riordan CM, Despali G, Vegetti S, Lovell MR, Moliné Á (2023) Sensitivity of strong lensing observations to dark matter substructure: a case study with Euclid. Mon Not R Astron Soc 521(2):2342–2356. https://doi.org/10.1093/mnras/stad650

Ostdiek B, Diaz Rivero A, Dvorkin C (2020) Extracting the Subhalo Mass Function from Strong Lens Images with Image Segmentation. Astrophys J 927:83. https://doi.org/10.3847/1538-4357/ac2d8d

Ostdiek B, Diaz Rivero A, Dvorkin C (2022) Image segmentation for analyzing galaxy-galaxy strong lensing systems. Astron Astrophys 657:14. https://doi.org/10.1051/0004-6361/202142030

Paduroiu S (2022) Warm dark matter in simulations. Universe 8(2):76. https://doi.org/10.3390/universe8020076

Patnaik AR, Browne IWA, Wilkinson PN, Wrobel JM (1992) Interferometer phase calibration sources - I. The region $35° \leq \delta \leq 75°$. Mon Not R Astron Soc 254:655. https://doi.org/10.1093/mnras/254.4.655

Pearson TJ, Readhead ACS (1984) Image formation by self-calibration in radio astronomy. Annu Rev Astron Astrophys 22:97–130. https://doi.org/10.1146/annurev.aa.22.090184.000525

Perreault Levasseur L, Hezaveh YD, Wechsler RH (2017) Uncertainties in parameters estimated with neural networks: application to strong gravitational lensing. Astrophys J Lett 850(1):7. https://doi.org/10.3847/2041-8213/aa9704

Petrillo CE, Tortora C, Vernardos G, Koopmans LVE, Verdoes Kleijn G, Bilicki M, Napolitano NR, Chatterjee S, Covone G, Dvornik A, Erben T, Getman F, Giblin B, Heymans C, de Jong JTA, Kuijken K, Schneider P, Shan H, Spiniello C, Wright AH (2019) LinKS: discovering galaxy-scale strong lenses in the kilo-degree survey using convolutional neural networks. Mon Not R Astron Soc 484(3):3879–3896. https://doi.org/10.1093/mnras/stz189

Pillepich A, Springel V, Nelson D, Genel S, Naiman J, Pakmor R, Hernquist L, Torrey P, Vogelsberger M, Weinberger R, Marinacci F (2018) Simulating galaxy formation with the IllustrisTNG model. Mon Not R Astron Soc 473(3):4077–4106. https://doi.org/10.1093/mnras/stx2656

Planck Collaboration, Aghanim N et al (2020a) Planck 2018 results. I. Overview and the cosmological legacy of Planck. Astron Astrophys 641:1. https://doi.org/10.1051/0004-6361/201833880

Planck Collaboration, Aghanim N et al (2020b) Planck 2018 results. VI. Cosmological parameters. Astron Astrophys 641:6. https://doi.org/10.1051/0004-6361/201833910

Portillo SKN, Lee BCG, Daylan T, Finkbeiner DP (2017) Improved point-source detection in crowded fields using probabilistic cataloging. Astron J 154(4):132. https://doi.org/10.3847/1538-3881/aa8565

Powell D, Vegetti S, McKean JP, Spingola C, Rizzo F, Stacey HR (2021) A novel approach to visibility-space modelling of interferometric gravitational lens observations at high angular resolution. Mon Not R Astron Soc 501(1):515–530. https://doi.org/10.1093/mnras/staa2740

Powell DM, Vegetti S, McKean JP, Spingola C, Stacey HR, Fassnacht CD (2022) A lensed radio jet at milliarcsecond resolution I: Bayesian comparison of parametric lens models. Mon Not R Astron Soc 516(2):1808–1828. https://doi.org/10.1093/mnras/stac2350

Powell DM, Vegetti S, McKean JP, White SDM, Ferreira EGM, May S, Spingola C (2023) A lensed radio jet at milli-arcsecond resolution II: Constraints on fuzzy dark matter from an extended gravitational arc. ArXiv e-prints, 2302–10941 https://doi.org/10.48550/arXiv.2302.10941

Press WH, Schechter P (1974) Formation of galaxies and clusters of galaxies by self-similar gravitational condensation. Astrophys J 187:425–438. https://doi.org/10.1086/152650
Press WH, Teukolsky SA, Vetterling WT, Flannery BP (1992) Numerical recipes in C. The art of scientific computing
Rezaei S, McKean JP, Biehl M, de Roo W, Lafontaine A (2022) A machine learning based approach to gravitational lens identification with the international LOFAR telescope. Mon Not R Astron Soc 517(1):1156–1170. https://doi.org/10.1093/mnras/stac2078
Richardson TRG, Stücker J, Angulo RE, Hahn O (2022) Non-halo structures and their effects on gravitational lensing. Mon Not R Astron Soc 511(4):6019–6032. https://doi.org/10.1093/mnras/stac493
Ritondale E, Auger MW, Vegetti S, McKean JP (2019b) Resolving on 100 pc scales the UV-continuum in Lyman-α emitters between redshift 2 and 3 with gravitational lensing. Mon Not R Astron Soc 482(4):4744–4762. https://doi.org/10.1093/mnras/sty2833
Ritondale E, Vegetti S, Despali G, Auger MW, Koopmans LVE, McKean JP (2019a) Low-mass halo perturbations in strong gravitational lenses at redshift z $\sim$ 0.5 are consistent with CDM. Mon Not R Astron Soc 485(2):2179–2193. https://doi.org/10.1093/mnras/stz464
Rizzo F, Vegetti S, Fraternali F, Di Teodoro E (2018) A novel 3D technique to study the kinematics of lensed galaxies. Mon Not R Astron Soc 481(4):5606–5629. https://doi.org/10.1093/mnras/sty2594
Robertson A, Massey R, Eke V, Tulin S, Yu H-B, Bahé Y, Barnes DJ, Bower RG, Crain RA, Dalla Vecchia C, Kay ST, Schaller M, Schaye J (2018) The diverse density profiles of galaxy clusters with self-interacting dark matter plus baryons. Mon Not R Astron Soc 476:20–24. https://doi.org/10.1093/mnrasl/sly024
Robertson A, Harvey D, Massey R, Eke V, McCarthy IG, Jauzac M, Li B, Schaye J (2019) Observable tests of self-interacting dark matter in galaxy clusters: cosmological simulations with SIDM and baryons. Mon Not R Astron Soc 488(3):3646–3662. https://doi.org/10.1093/mnras/stz1815
Robertson A, Massey R, Eke V, Schaye J, Theuns T (2021) The surprising accuracy of isothermal jeans modelling of self-interacting dark matter density profiles. Mon Not R Astron Soc 501(3):4610–4634. https://doi.org/10.1093/mnras/staa3954
Rocha M, Peter AHG, Bullock JS, Kaplinghat M, Garrison-Kimmel S, Oñorbe J, Moustakas LA (2013) Cosmological simulations with self-interacting dark matter - I. Constant-density cores and substructure. Mon Not R Astron Soc 430:81–104. https://doi.org/10.1093/mnras/sts514
Rubin DB (1984) Bayesianly justifiable and relevant frequency calculations for the applied statistician. Ann Stat 12. https://doi.org/10.1214/aos/1176346785
Rubin VC (1991) Evidence for dark matter from rotation curves: ten years later. In: Holt SS, Bennett CL, Trimble V (eds) After the first three minutes. AIP Conference Proceedings, vol 222, pp 371–380. https://doi.org/10.1063/1.40398
Rybak M, McKean JP, Vegetti S, Andreani P, White SDM (2015) ALMA imaging of SDP.81 - I. A pixelated reconstruction of the far-infrared continuum emission. Mon Not R Astron Soc 451:40–44. https://doi.org/10.1093/mnrasl/slv058
Sagunski L, Gad-Nasr S, Colquhoun B, Robertson A, Tulin S (2021) Velocity-dependent self-interacting dark matter from groups and clusters of galaxies. J Cosmol Astropart Phys 2021(1):024. https://doi.org/10.1088/1475-7516/2021/01/024
Sameie O, Creasey P, Yu H-B, Sales LV, Vogelsberger M, Zavala J (2018) The impact of baryonic discs on the shapes and profiles of self-interacting dark matter haloes. Mon Not R Astron Soc 479:359–367. https://doi.org/10.1093/mnras/sty1516
Sameie O, Yu H-B, Sales LV, Vogelsberger M, Zavala J (2020) Self-interacting dark matter subhalos in the Milky Way's tides. Phys Rev Lett 124(14):141102. https://doi.org/10.1103/PhysRevLett.124.141102
Sawala T, Frenk CS, Fattahi A, Navarro JF, Bower RG, Crain RA, Dalla Vecchia C, Furlong M, Jenkins A, McCarthy IG, Qu Y, Schaller M, Schaye J, Theuns T (2015) Bent by baryons: the low-mass galaxy-halo relation. Mon Not R Astron Soc 448:2941–2947. https://doi.org/10.1093/mnras/stu2753
Sawala T, Pihajoki P, Johansson PH, Frenk CS, Navarro JF, Oman KA, White SDM (2017) Shaken and stirred: the Milky Way's dark substructures. Mon Not R Astron Soc 467:4383–4400. https://doi.org/10.1093/mnras/stx360
Schaye J, Crain RA, Bower RG, Furlong M, Schaller M, Theuns T, Dalla Vecchia C, Frenk CS et al (2015) The EAGLE project: simulating the evolution and assembly of galaxies and their environments. Mon Not R Astron Soc 446:521–554. https://doi.org/10.1093/mnras/stu2058
Schive H-Y, Chiueh T, Broadhurst T (2014a) Cosmic structure as the quantum interference of a coherent dark wave. Nat Phys 10(7):496–499. https://doi.org/10.1038/nphys2996
Schive H-Y, Liao M-H, Woo T-P, Wong S-K, Chiueh T, Broadhurst T, Hwang W-YP (2014b) Understanding the core-halo relation of quantum wave dark matter from 3D simulations. Phys Rev Lett 113(26):261302. https://doi.org/10.1103/PhysRevLett.113.261302
Schive H-Y, Chiueh T, Broadhurst T, Huang K-W (2016) Contrasting galaxy formation from quantum wave dark matter, ψDM, with ΛCDM, using Planck and Hubble data. Astrophys J 818(1):89. https://doi.org/10.3847/0004-637X/818/1/89

Schneider A (2015) Structure formation with suppressed small-scale perturbations. Mon Not R Astron Soc 451(3):3117–3130. https://doi.org/10.1093/mnras/stv1169

Schneider A, Smith RE, Macciò AV, Moore B (2012) Non-linear evolution of cosmological structures in warm dark matter models. Mon Not R Astron Soc 424:684–698. https://doi.org/10.1111/j.1365-2966.2012.21252.x

Schuldt S, Suyu SH, Meinhardt T, Leal-Taixé L, Cañameras R, Taubenberger S, Halkola A (2021) HOLISMOKES. IV. Efficient mass modeling of strong lenses through deep learning. Astron Astrophys 646:126. https://doi.org/10.1051/0004-6361/202039574

Şengül AÇ, Dvorkin C (2022) Probing dark matter with strong gravitational lensing through an effective density slope. Mon Not R Astron Soc 516(1):336–357. https://doi.org/10.1093/mnras/stac2256

Sengül AÇ, Dvorkin C, Ostdiek B, Tsang A (2022) Substructure detection reanalysed: dark perturber shown to be a line-of-sight halo. Mon Not R Astron Soc 515(3):4391–4401. https://doi.org/10.1093/mnras/stac1967

Shajib AJ, Vernardos G, Collett TE, Motta V, Sluse D, Williams LLR, Saha P, Birrer S, Spiniello C, Treu T (2024) Space Sci Rev 220

Shen X, Brinckmann T, Rapetti D, Vogelsberger M, Mantz A, Zavala J, Allen SW (2022) X-ray morphology of cluster-mass haloes in self-interacting dark matter. Mon Not R Astron Soc 516(1):1302–1319. https://doi.org/10.1093/mnras/stac2376

Sheth RK, Lemson G (1999) The forest of merger history trees associated with the formation of dark matter haloes. Mon Not R Astron Soc 305(4):946–956. https://doi.org/10.1046/j.1365-8711.1999.02477.x

Sheth RK, Tormen G (1999) Large-scale bias and the peak background split. Mon Not R Astron Soc 308(1):119–126. https://doi.org/10.1046/j.1365-8711.1999.02692.x

Sheth RK, Mo HJ, Tormen G (2001) Ellipsoidal collapse and an improved model for the number and spatial distribution of dark matter haloes. Mon Not R Astron Soc 323:1–12. https://doi.org/10.1046/j.1365-8711.2001.04006.x

Shu Y, Bolton AS, Mao S, Kochanek CS, Pérez-Fournon I, Oguri M, Montero-Dorta AD, Cornachione MA, Marques-Chaves R, Zheng Z, Brownstein JR, Ménard B (2016) The BOSS emission-line lens survey. IV. Smooth lens models for the BELLS GALLERY sample. Astrophys J 833(2):264. https://doi.org/10.3847/1538-4357/833/2/264

Smirnov OM (2011) Revisiting the radio interferometer measurement equation. I. A full-sky Jones formalism. Astron Astrophys 527:106. https://doi.org/10.1051/0004-6361/201016082

Song Y, Sohl-Dickstein J, Kingma DP, Kumar A, Ermon S, Poole B (2020) Score-Based Generative Modeling through Stochastic Differential Equations. ArXiv e-prints, arXiv:2011.13456 [cs.LG]. https://doi.org/10.48550/arXiv.2011.13456

Sonnenfeld A (2022) Statistical strong lensing. III. Inferences with complete samples of lenses. Astron Astrophys 659:132. https://doi.org/10.1051/0004-6361/202142301

Sonnenfeld A, Tortora C, Hoekstra H, Asgari M, Bilicki M, Heymans C, Hildebrandt H, Kuijken K, Napolitano NR, Roy N, Valentijn E, Wright AH (2022) The dark matter halo masses of elliptical galaxies as a function of observationally robust quantities. Astron Astrophys 662:55. https://doi.org/10.1051/0004-6361/202142511

Spilker JS, Marrone DP, Aravena M, Béthermin M, Bothwell MS, Carlstrom JE, Chapman SC, Crawford TM, de Breuck C, Fassnacht CD, Gonzalez AH, Greve TR, Hezaveh Y, Litke K, Ma J, Malkan M, Rotermund KM, Strandet M, Vieira JD, Weiss A, Welikala N (2016) ALMA imaging and gravitational lens models of south pole telescope—selected dusty, star-forming galaxies at high redshifts. Astrophys J 826(2):112. https://doi.org/10.3847/0004-637X/826/2/112

Spingola C, Barnacka A (2020) Constraining VLBI-optical offsets in high redshift galaxies using strong gravitational lensing. Mon Not R Astron Soc 494(2):2312–2326. https://doi.org/10.1093/mnras/staa870

Spingola C, McKean JP, Auger MW, Fassnacht CD, Koopmans LVE, Lagattuta DJ, Vegetti S (2018) SHARP - V. Modelling gravitationally lensed radio arcs imaged with global VLBI observations. Mon Not R Astron Soc 478(4):4816–4829. https://doi.org/10.1093/mnras/sty1326

Spingola C, McKean JP, Lee M, Deller A, Moldon J (2019) A novel search for gravitationally lensed radio sources in wide-field VLBI imaging from the mJIVE-20 survey. Mon Not R Astron Soc 483(2):2125–2153. https://doi.org/10.1093/mnras/sty3189

Springel V, White SDM, Jenkins A, Frenk CS, Yoshida N, Gao L, Navarro J, Thacker R, Croton D, Helly J, Peacock JA, Cole S, Thomas P, Couchman H, Evrard A, Colberg J, Pearce F (2005) Simulations of the formation, evolution and clustering of galaxies and quasars. Nature 435(7042):629–636. https://doi.org/10.1038/nature03597

Springel V, Wang J, Vogelsberger M, Ludlow A, Jenkins A, Helmi A, Navarro JF, Frenk CS, White SDM (2008) The aquarius project: the subhaloes of galactic haloes. Mon Not R Astron Soc 391(4):1685–1711. https://doi.org/10.1111/j.1365-2966.2008.14066.x

Stacey HR, McKean JP, Powell DM, Vegetti S, Rizzo F, Spingola C, Auger MW, Ivison RJ, van der Werf PP (2021) The rocky road to quiescence: compaction and quenching of quasar host galaxies at z ∼ 2. Mon Not R Astron Soc 500(3):3667–3688. https://doi.org/10.1093/mnras/staa3433

Storfer C, Huang X, Gu A, Sheu W, Banka S, Dey A, Jain A, Kwon J, Lang D, Lee V, Meisner A, Moustakas J, Myers AD, Tabares-Tarquinio S, Schlafly EF, Schlegel DJ (2022) New Strong Gravitational Lenses from the DESI Legacy Imaging Surveys Data Release 9. ArXiv e-prints, arXiv:2206.02764 [astro-ph.CO]. https://doi.org/10.48550/arXiv.2206.02764

Stücker J, Hahn O, Angulo RE, White SDM (2020) Simulating the complexity of the dark matter sheet I: numerical algorithms. Mon Not R Astron Soc 495(4):4943–4964. https://doi.org/10.1093/mnras/staa1468

Suyu SH, Marshall PJ, Hobson MP, Blandford RD (2006) A Bayesian analysis of regularized source inversions in gravitational lensing. Mon Not R Astron Soc 371(2):983–998. https://doi.org/10.1111/j.1365-2966.2006.10733.x

Suyu SH, Marshall PJ, Blandford RD, Fassnacht CD, Koopmans LVE, McKean JP, Treu T (2009) Dissecting the gravitational lens B1608+656. I. Lens potential reconstruction. Astrophys J 691(1):277–298. https://doi.org/10.1088/0004-637X/691/1/277

Tagore AS, Keeton CR (2014) Statistical and systematic uncertainties in pixel-based source reconstruction algorithms for gravitational lensing. Mon Not R Astron Soc 445(1):694–710. https://doi.org/10.1093/mnras/stu1671

Tavaré S, Balding DJ, Griffiths RC, Donnelly P (1997) Inferring coalescence times from DNA sequence data. Genetics 145(2):505–518. https://doi.org/10.1093/genetics/145.2.505

Tie SS, Kochanek CS (2018) Microlensing makes lensed quasar time delays significantly time variable. Mon Not R Astron Soc 473(1):80–90. https://doi.org/10.1093/mnras/stx2348

Tinker J, Kravtsov AV, Klypin A, Abazajian K, Warren M, Yepes G, Gottlöber S, Holz DE (2008) Toward a halo mass function for precision cosmology: the limits of universality. Astrophys J 688:709–728. https://doi.org/10.1086/591439

Treu T, Koopmans LVE (2004) Massive dark matter halos and evolution of early-type galaxies to $z \approx 1$. Astrophys J 611(2):739–760. https://doi.org/10.1086/422245

Trotter CS, Winn JN, Hewitt JN (2000) A multipole-Taylor expansion for the potential of the gravitational lens MG J0414+0534. Astrophys J 535(2):671–691. https://doi.org/10.1086/308861

Turner B, Van Zandt T (2012) A tutorial on approximate Bayesian computation. J Math Psychol 56:69–85. https://doi.org/10.1016/j.jmp.2012.02.005

Turner HC, Lovell MR, Zavala J, Vogelsberger M (2021) The onset of gravothermal core collapse in velocity-dependent self-interacting dark matter subhaloes. Mon Not R Astron Soc 505(4):5327–5339. https://doi.org/10.1093/mnras/stab1725

van Albada TS, Bahcall JN, Begeman K, Sancisi R (1985) Distribution of dark matter in the spiral galaxy NGC 3198. Astrophys J 295:305–313. https://doi.org/10.1086/163375

Van de Vyvere L, Gomer MR, Sluse D, Xu D, Birrer S, Galan A, Vernardos G (2022) TDCOSMO. VII. Boxyness/discyness in lensing galaxies: detectability and impact on H_0. Astron Astrophys 659:127. https://doi.org/10.1051/0004-6361/202141551

Varma S, Fairbairn M, Figueroa J (2020) Dark matter subhalos, strong lensing and machine learning. ArXiv e-prints, arXiv:2005.05353 [astro-ph.CO]. https://doi.org/10.48550/arXiv.2005.05353

Vattis K, Toomey MW, Koushiappas SM (2021) Deep learning the astrometric signature of dark matter substructure. Phys Rev D 104(12):123541. https://doi.org/10.1103/PhysRevD.104.123541

Vegetti S, Koopmans LVE (2009) Bayesian strong gravitational-lens modelling on adaptive grids: objective detection of mass substructure in galaxies. Mon Not R Astron Soc 392(3):945–963. https://doi.org/10.1111/j.1365-2966.2008.14005.x

Vegetti S, Koopmans LVE (2009) Statistics of mass substructure from strong gravitational lensing: quantifying the mass fraction and mass function. Mon Not R Astron Soc 400(3):1583–1592. https://doi.org/10.1111/j.1365-2966.2009.15559.x

Vegetti S, Czoske O, Koopmans LVE (2010) Quantifying dwarf satellites through gravitational imaging: the case of SDSSJ120602.09+514229.5. Mon Not R Astron Soc 407(1):225–231. https://doi.org/10.1111/j.1365-2966.2010.16952.x

Vegetti S, Koopmans LVE, Bolton A, Treu T, Gavazzi R (2010) Detection of a dark substructure through gravitational imaging. Mon Not R Astron Soc 408(4):1969–1981. https://doi.org/10.1111/j.1365-2966.2010.16865.x

Vegetti S, Lagattuta DJ, McKean JP, Auger MW, Fassnacht CD, Koopmans LVE (2012) Gravitational detection of a low-mass dark satellite galaxy at cosmological distance. Nature 481(7381):341–343. https://doi.org/10.1038/nature10669

Vegetti S, Koopmans LVE, Auger MW, Treu T, Bolton AS (2014) Inference of the cold dark matter substructure mass function at z = 0.2 using strong gravitational lenses. Mon Not R Astron Soc 442(3):2017–2035. https://doi.org/10.1093/mnras/stu943

Vegetti S, Despali G, Lovell MR, Enzi W (2018) Constraining sterile neutrino cosmologies with strong gravitational lensing observations at redshift z ∼ 0.2. Mon Not R Astron Soc 481(3):3661–3669. https://doi.org/10.1093/mnras/sty2393

Vernardos G, Koopmans LVE (2022) The very knotty lenser: exploring the role of regularization in source and potential reconstructions using Gaussian process regression. Mon Not R Astron Soc 516(1):1347–1372. https://doi.org/10.1093/mnras/stac1924

Vernardos G, Tsagkatakis G, Pantazis Y (2020) Quantifying the structure of strong gravitational lens potentials with uncertainty-aware deep neural networks. Mon Not R Astron Soc 499(4):5641–5652. https://doi.org/10.1093/mnras/staa3201

Viel M, Markovič K, Baldi M, Weller J (2012) The non-linear matter power spectrum in warm dark matter cosmologies. Mon Not R Astron Soc 421(1):50–62. https://doi.org/10.1111/j.1365-2966.2011.19910.x

Villasenor B, Robertson B, Madau P, Schneider E (2023) New Constraints on Warm Dark Matter from the Lyman-α Forest Power Spectrum. Phys Rev D 108:023502. https://doi.org/10.1103/PhysRevD.108.023502

Vogelsberger M, Zavala J, Loeb A (2012) Subhaloes in self-interacting galactic dark matter haloes. Mon Not R Astron Soc 423:3740–3752. https://doi.org/10.1111/j.1365-2966.2012.21182.x

Vogelsberger M, Genel S, Springel V, Torrey P, Sijacki D, Xu D, Snyder G, Nelson D, Hernquist L (2014b) Introducing the illustris project: simulating the coevolution of dark and visible matter in the universe. Mon Not R Astron Soc 444:1518–1547. https://doi.org/10.1093/mnras/stu1536

Vogelsberger M, Zavala J, Simpson C, Jenkins A (2014a) Dwarf galaxies in CDM and SIDM with baryons: observational probes of the nature of dark matter. Mon Not R Astron Soc 444:3684–3698. https://doi.org/10.1093/mnras/stu1713

Vogelsberger M, Zavala J, Cyr-Racine F-Y, Pfrommer C, Bringmann T, Sigurdson K (2016) ETHOS - an effective theory of structure formation: dark matter physics as a possible explanation of the small-scale CDM problems. Mon Not R Astron Soc 460:1399–1416. https://doi.org/10.1093/mnras/stw1076

Vogelsberger M, Zavala J, Schutz K, Slatyer TR (2019) Evaporating the Milky Way halo and its satellites with inelastic self-interacting dark matter. Mon Not R Astron Soc 484(4):5437–5452. https://doi.org/10.1093/mnras/stz340

Wagner-Carena S, Aalbers J, Birrer S, Nadler EO, Darragh-Ford E, Marshall PJ, Wechsler RH (2023) From images to dark matter: end-to-end inference of substructure from hundreds of strong gravitational lenses. Astrophys J 942(2):75. https://doi.org/10.3847/1538-4357/aca525

Warren SJ, Dye S (2003) Semilinear gravitational lens inversion. Astrophys J 590(2):673–682. https://doi.org/10.1086/375132

White SDM, Frenk CS, Davis M (1983) Clustering in a neutrino-dominated universe. Astrophys J Lett 274:1–5. https://doi.org/10.1086/184139

Wilkinson PN, Browne IWA, Patnaik AR, Wrobel JM, Sorathia B (1998) Interferometer phase calibration sources - III. The regions $+20 \leq \delta_{\mathrm{B1950}} \leq +35°$ and $+75 \leq \delta_{\mathrm{B1950}} \leq +90°$. Mon Not R Astron Soc 300(3):790–816. https://doi.org/10.1046/j.1365-8711.1998.01941.x

Wizinowich P, Lu JR, Cetre S, Chin J, Correia C, Delorme J-R, Gers L, Lilley S, Lyke J, Marin E, Ragland S, Richards P, Surendran A, Wetherell E, Chen C-F, Chu D, Do T, Fassnacht C, Freeman M, Gautam A, Ghez A, Hunter L, Jones T, Liu MC, Mawet D, Max C, Morris M, Phillips M, Ruffio J-B, Rundquist N-E, Sabhlok S, Terry S, Treu T, Wright S (2022) Keck all sky precision adaptive optics program overview. In: Schreiber L, Schmidt D, Vernet E (eds) Adaptive optics systems VIII. Society of Photo-Optical Instrumentation Engineers (SPIE) conference series, vol 12185, p 121850. https://doi.org/10.1117/12.2628275

Wucknitz O (2004) LENSCLEAN revisited. Mon Not R Astron Soc 349(1):1–13. https://doi.org/10.1111/j.1365-2966.2004.07513.x

Xu DD, Mao S, Wang J, Springel V, Gao L, White SDM, Frenk CS, Jenkins A, Li G, Navarro JF (2009) Effects of dark matter substructures on gravitational lensing: results from the Aquarius simulations. Mon Not R Astron Soc 398(3):1235–1253. https://doi.org/10.1111/j.1365-2966.2009.15230.x

Xu DD, Mao S, Cooper AP, Wang J, Gao L, Frenk CS, Springel V (2010) Substructure lensing: effects of galaxies, globular clusters and satellite streams. Mon Not R Astron Soc 408(3):1721–1729. https://doi.org/10.1111/j.1365-2966.2010.17235.x

Xu DD, Mao S, Cooper AP, Gao L, Frenk CS, Angulo RE, Helly J (2012) On the effects of line-of-sight structures on lensing flux-ratio anomalies in a ΛCDM universe. Mon Not R Astron Soc 421(3):2553–2567. https://doi.org/10.1111/j.1365-2966.2012.20484.x

Xu D, Sluse D, Gao L, Wang J, Frenk C, Mao S, Schneider P, Springel V (2015) How well can cold dark matter substructures account for the observed radio flux-ratio anomalies. Mon Not R Astron Soc 447(4):3189–3206. https://doi.org/10.1093/mnras/stu2673

Yang D, Nadler EO, Yu H-B (2023) Strong dark matter self-interactions diversify halo populations within and surrounding the Milky Way. Astrophys J 949:67. https://doi.org/10.3847/1538-4357/acc73e

Yao-Yu Lin J, Yu H, Morningstar W, Peng J, Holder G (2020) Hunting for Dark Matter Subhalos in Strong Gravitational Lensing with Neural Networks. ArXiv e-prints, arXiv:2010.12960 [astro-ph.CO]. https://doi.org/10.48550/arXiv.2010.12960

Yavetz TD, Li X, Hui L (2022) Construction of wave dark matter halos: numerical algorithm and analytical constraints. Phys Rev D 105(2):023512. https://doi.org/10.1103/PhysRevD.105.023512

Zavala J, Frenk CS (2019) Dark matter haloes and subhaloes. Galaxies 7(4):81. https://doi.org/10.3390/galaxies7040081

Zel'dovich YB (1970) Gravitational instability: an approximate theory for large density perturbations. Astron Astrophys 5:84–89

Zelko IA, Treu T, Abazajian KN, Gilman D, Benson AJ, Birrer S, Nierenberg AM, Kusenko A (2022) Constraints on sterile neutrino models from strong gravitational lensing, Milky Way satellites, and the Lyman-α forest. Phys Rev Lett 129(19):191301. https://doi.org/10.1103/PhysRevLett.129.191301

Zeng ZC, Peter AHG, Du X, Benson A, Kim S, Jiang F, Cyr-Racine F-Y, Vogelsberger M (2022) Core-collapse, evaporation, and tidal effects: the life story of a self-interacting dark matter subhalo. Mon Not R Astron Soc 513(4):4845–4868. https://doi.org/10.1093/mnras/stac1094

Zentner AR, Bullock JS (2003) Halo substructure and the power spectrum. Astrophys J 598(1):49–72. https://doi.org/10.1086/378797

Zwicky F (1933) Die Rotverschiebung von extragalaktischen Nebeln. Helv Phys Acta 6:110–127

Authors and Affiliations

S. Vegetti[1] · S. Birrer[2] · G. Despali[3,4] · C.D. Fassnacht[5] · D. Gilman[6] · Y. Hezaveh[7,8,9,10,11] · L. Perreault Levasseur[7,8,9,10,11] · J.P. McKean[12,13,14] · D.M. Powell[1] · C.M. O'Riordan[1] · G. Vernardos[15]

✉ S. Vegetti
svegetti@mpa-garching.mpg.de

1 Max Planck Institut für Astrophysik, Karl-Schwarzschild-Strasse 1, D-85748 Garching bei München, Germany

2 Department of Physics and Astronomy, Stony Brook University, Stony Brook, NY 11794, USA

3 Dipartimento di Fisica e Astronomia "A. Righi", Alma Mater Studiorum Università di Bologna, Via Piero Gobetti 93/2, I-40129 Bologna, Italy

4 Institut für Theoretische Astrophysik, Zentrum für Astronomie, Heidelberg Universität, Albert-Ueberle-Str. 2, 69120, Heidelberg, Germany

5 Dept. of Physics and Astronomy, University of California, Davis, 1 Shields Ave. Davis, CA 95616, USA

6 Department of Astronomy and Astrophysics, University of Toronto, Toronto, ON, M5S 3H4, Canada

7 Department of Physics, Université de Montréal, Montréal, Canada

8 Mila - Quebec Artificial Intelligence Institute, Montréal, Canada

9 Ciela - Montreal Institute for Astrophysical Data Analysis and Machine Learning, Montréal, Canada

10 Center for Computational Astrophysics, Flatiron Institute, 162 5th Avenue, 10010, New York, NY, USA

11 Perimeter Institute for Theoretical Physics, Waterloo, Ontario, Canada, N2L 2Y5

[12] Kapteyn Astronomical Institute, University of Groningen, PO Box 800, NL-9700 AV Groningen, The Netherlands

[13] South African Radio Astronomy Observatory (SARAO), P.O. Box 443, Krugersdorp 1740, South Africa

[14] Department of Physics, University of Pretoria, Lynnwood Road, Hatfield, Pretoria, 0083, South Africa

[15] Institute of Physics, Laboratory of Astrophysique, École Polytechnique Fédérale de Lausanne (EPFL), Observatoire de Sauverny, 1290 Versoix, Switzerland